LETTER

doi:10.1038/nature21706

# The lung is a site of platelet biogenesis and a reservoir for haematopoietic progenitors

Emma Lefrançais[1]*, Guadalupe Ortiz-Muñoz[1]*, Axelle Caudrillier[1], Beñat Mallavia[1], Fengchun Liu[1], David M. Sayah[2], Emily E. Thornton[3], Mark B. Headley[3], Tovo David[4], Shaun R. Coughlin[4], Matthew F. Krummel[3], Andrew D. Leavitt[1], Emmanuelle Passegué[1] & Mark R. Looney[1,5]

**Platelets are critical for haemostasis, thrombosis, and inflammatory responses[1,2], but the events that lead to mature platelet production remain incompletely understood[3]. The bone marrow has been proposed to be a major site of platelet production, although there is indirect evidence that the lungs might also contribute to platelet biogenesis[4–7]. Here, by directly imaging the lung microcirculation in mice[8], we show that a large number of megakaryocytes circulate through the lungs, where they dynamically release platelets. Megakaryocytes that release platelets in the lungs originate from extrapulmonary sites such as the bone marrow; we observed large megakaryocytes migrating out of the bone marrow space. The contribution of the lungs to platelet biogenesis is substantial, accounting for approximately 50% of total platelet production or 10 million platelets per hour. Furthermore, we identified populations of mature and immature megakaryocytes along with haematopoietic progenitors in the extravascular spaces of the lungs. Under conditions of thrombocytopenia and relative stem cell deficiency in the bone marrow[9], these progenitors can migrate out of the lungs, repopulate the bone marrow, completely reconstitute blood platelet counts, and contribute to multiple haematopoietic lineages. These results identify the lungs as a primary site of terminal platelet production and an organ with considerable haematopoietic potential.**

Platelets are released from megakaryocytes; however, even though they were discovered in the nineteenth century, we do not completely understand the mechanisms by which platelets are produced. On the basis of previous work showing the presence of megakaryocytes in the lungs[10] and demonstrating that blood leaving the lungs contains more platelets and fewer megakaryocytes than blood entering the lungs[4,11], we hypothesized that the lungs could have a major role in platelet biogenesis, and directly investigated this process using 2-photon intravital microscopy (2PIVM) of the lungs and fluorescent reporter mouse strains. We used PF4-Cre × *Gt(ROSA)26Sor*$^{tm4(ACTB-tdTomato,-EGFP)Luo}$ (mTmG) (hereafter called PF4-mTmG) reporter mice, in which PF4-Cre[12] drives membrane GFP expression in megakaryocytes and platelets, while all other cells are labelled with membrane tomato. We observed large circulating GFP$^+$ cells that passed through the lung microcirculation, where they produced GFP$^+$ extensions in a flow-dependent manner (Fig. 1a, b and Supplementary Video 1). These events resembled proplatelet and preplatelet formation from cultured megakaryocytes[3,13,14]. In the lungs, the duration of these events varied from approximately 20 to 60 min (Fig. 1a, b and Supplementary Video 1). Many of the GFP$^+$ cells contained large nuclei (more than 10 μm), which appeared as unlabelled dark holes that remained intact during this process (Fig. 1b and Supplementary Video 2) and resulted in naked intravascular nuclei after platelets were released (Supplementary Video 2). We confirmed that we labelled large mobile nucleated cells by imaging the lung microcirculation of PF4-Cre × *Gt(ROSA)26Sor*$^{tm1(CAG-tdTomato*,-EGFP*)Ees}$ (nTnG) (hereafter called PF4-nTnG) reporter mice, in which a fluorescence switch allows GFP$^+$ nuclei to be tracked (Extended Data Fig. 1a and Supplementary Video 3).

We next quantified the GFP$^+$ megakaryocytes and proplatelets in PF4-mTmG lungs by assigning surface volumes (Fig. 1c and Supplementary Video 4). The putative megakaryocytes (large GFP$^+$ cells undergoing platelet release) had median volumes of 10,000 $\mu m^3$ and diameters of more than 25 μm (Fig. 1d, e), whereas the putative platelets (small circulating GFP$^+$ events) had median volumes of below 10 $\mu m^3$ and diameters of 2–3 μm (Fig. 1d, e). These values are consistent with previous estimates of megakaryocytes and platelet sizes[3]. For each large GFP$^+$ cell undergoing platelet release, we calculated the number of platelets that could be liberated into the lung circulation, and this ranged from fewer than 500 platelets for small megakaryocytes or proplatelets to more than 1,000 platelets for larger megakaryocytes (Fig. 1f), with a median of around 500 platelets per megakaryocyte. Previous studies have produced widely varying estimates of the number of platelets produced from a single megakaryocyte (200–10,000 platelets)[15–17]. Our method uses direct measurement for each event, and therefore is likely to yield more accurate estimates. In total, we analysed 20 h of footage from 10 mice, and observed an average of $2.2 \pm 0.26$ ($n = 10$) megakaryocytes per hour in an imaged lung volume of 0.07 $mm^3$ (Fig. 1g and Supplementary Video 5). When extrapolated to the entire lung volume, this equals more than 10 million platelets produced per hour from the lungs (Fig. 1h, Methods and Extended Data Table 1). Overall, when adjusted for platelet lifespan and splenic sequestration, we estimate that the lung is responsible for approximately 50% of total platelet production in the mouse (Fig. 1i, Methods and Extended Data Table 1). Blood platelet counts were unchanged after 2PIVM (Extended Data Fig. 1b). Platelet production by the lungs is also biologically tunable, as the administration of the megakaryocyte growth factor thrombopoietin (TPO) increased blood platelets threefold (Fig. 1j) and the number of megakaryocytes undergoing proplatelet formation observed per hour twofold ($3.9 \pm 0.38$, $n = 9$) (Fig. 1k). We conclude from these experiments that the lungs are a primary site of platelet biogenesis.

To investigate the origin of the intravascular megakaryocytes and proplatelets in the lungs, we adoptively transferred lung resident cells using the orthotopic single-lung transplant model in mice[18]. We transplanted a lung from an mTmG mouse (with no Cre or GFP expression) into a PF4-mTmG recipient mouse and vice versa (Extended Data Fig. 1c–e and Supplementary Video 6). Using 2PIVM, we observed proplatelet formation from GFP$^+$ megakaryocytes in the lung vasculature following transplantation of mTmG lungs to PF4-mTmG mice, but not following the reverse transplant (PF4-mTmG lungs to mTmG mice). These experiments confirmed that megakaryocytes releasing platelets in the lung circulation originate from outside the lungs.

[1]Department of Medicine, University of California, San Francisco (UCSF), San Francisco, California 94143, USA. [2]Department of Medicine, University of California, Los Angeles (UCLA), Los Angeles, California 90095, USA. [3]Department of Pathology, University of California, San Francisco (UCSF), San Francisco, California 94143, USA. [4]Cardiovascular Research Institute, University of California, San Francisco (UCSF), San Francisco, California 94143, USA. [5]Department of Laboratory Medicine, University of California, San Francisco (UCSF), San Francisco, California 94143, USA.
*These authors contributed equally to this work.

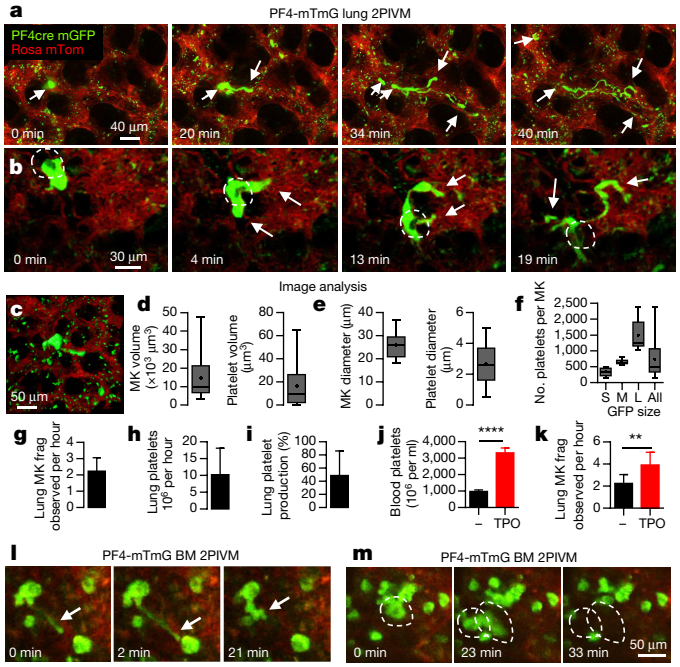


**Figure 1 | The lungs are an important site of megakaryocyte circulation and platelet production.** **a**–**c**, Visualization of megakaryocytes and platelet production in the lung circulation by 2PIVM in PF4-mTmG mice. **a**, **b**, Sequential images show a large megakaryocyte (green) in the lung capillaries (red) where it undergoes proplatelet formation (arrows). **b**, Dark hole in the cytoplasm (dashed outline) indicates the nucleus. Time elapsed is indicated. **c**–**f**, Characterization of PF4$^+$ events by image analysis. **c**, Representative image of surface analysis of the GFP channel. **d**, **e**, Volume distribution (**d**) and equivalent diameter (**e**) of megakaryocytes (MKs, $n = 35$) and platelets ($n = 492$). **f**, Number of platelets produced by one megakaryocyte according to its size: small (<500 platelets, $n = 18$), medium (500–1,000 platelets, $n = 7$) and large (>1,000 platelets, $n = 10$). **d**–**f**, Minimum-to-maximum boxplots are presented. **g**–**i**, Quantification of lung platelet production. **g**, Number of megakaryocytes releasing platelets observed per hour in imaged lung volume (2-h movies, $n = 10$). **h**, **i**, Estimation of the number (**h**) and the percentage (**i**) of platelets produced by the lung. **j**, **k**, Platelet counts in the blood (**j**) and number of megakaryocytes releasing platelets in the lungs (**k**) 5 days after TPO treatment. $n \geq 5$ mice per group. Unpaired *t*-test: $^{****}P < 0.0001$, $^{**}P < 0.005$. **g**–**k**, Mean ± s.d. are presented. **l**, **m**, Visualization of proplatelet release (arrow) and megakaryocyte migration (circled) in bone marrow (BM) sinusoids by 2PIVM in PF4-mTmG mice.

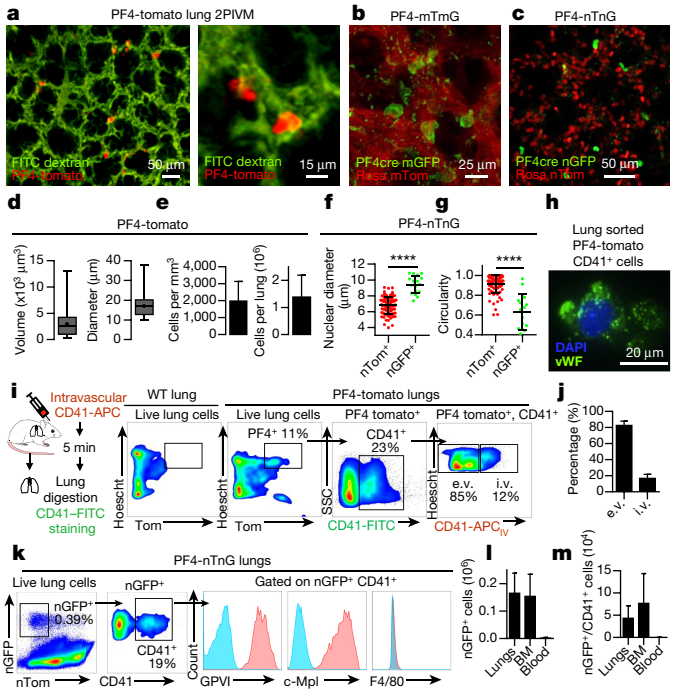


**Figure 2 | Resident megakaryocytes are present in the extravascular spaces of the lung.** **a**–**c**, Visualization of resident or static megakaryocytes in the lung by 2PIVM of PF4-tomato (**a**), PF4-mTmG (**b**), and PF4-nTnG mice (**c**). (**d**) Size characterization of PF4$^+$ cells (red, >10 µm) by quantitative image analysis of PF4-tomato lungs ($n = 312$). Minimum-to-maximum boxplots are presented. **e**, Quantification of PF4$^+$ cells (red, >10 µm) ($n = 6$). **f**, **g**, Comparison of nuclear size (**f**) and circularity (**g**) between PF4$^+$ cells (green, $n = 17$) and all other lung cells (red, $n = 91$) by quantitative image analysis of PF4-nTnG lungs. Unpaired *t*-test: $^{****}P < 0.0001$. **h**, Representative immunofluorescence images of PF4$^+$ and CD41$^+$ cells sorted from perfused PF4-tomato lungs and stained with anti-vWF antibodies (green) and 4′,6-diamidino-2-phenylindole (DAPI, blue). **i**, **j**, Intravascular (i.v.) or extravascular (e.v.) localization of PF4$^+$ and CD41–FITC$^+$ cells. **i**, Experimental schema and representative fluorescence-activated cell sorting (FACS) plots. **j**, Percentage of cells located intravascularly or extravascularly (mean of four experiments, $n = 8$ mice). **k**, FACS gating strategy and surface expression of nucleated PF4$^+$ and CD41$^+$ cells from lungs of PF4-nTnG mice. **l**, **m**, FACS quantification of nucleated PF4$^+$ (**l**) and nucleated PF4$^+$/CD41$^+$ (**m**) cells in PF4-nTnG whole lung ($n = 28$), bone marrow (BM, $n = 24$) (two femurs, two tibias × 6.6) and blood (1.5 ml, $n = 8$). **e**–**g**, **l**, **m**, Mean ± s.d. presented.

We hypothesized that the bone marrow[19], spleen, or liver could be the source of these intravascular megakaryocytes and proplatelets. We imaged the calvarial bone marrow (Extended Data Fig. 1f) and the spleen in PF4-mTmG mice and observed extravascular megakaryocytes releasing proplatelets into the sinusoids of the bone marrow (Fig. 1l, Extended Data Fig. 1g and Supplementary Video 7) and spleen (Extended Data Fig. 1i and Supplementary Video 9). We also observed large megakaryocytes exiting the bone marrow space (Fig. 1m and Supplementary Video 8). In contrast to observations in the lung, we did not observe any intravascular megakaryocytes undergoing proplatelet formation. We did not observe any megakaryocytes in the liver (Extended Data Fig. 1h).

In addition to intravascular megakaryocytes, we also observed large cells in the perivascular lung interstitium in PF4-Cre × *Gt(ROSA)26Sor*$^{tm9(CAG\text{-}tdTomato)Hze}$ (ROSA26-tdTomato) (hereafter called PF4-tomato) and PF4-mTmG mice (Fig. 2a, b, Extended Data Fig. 2a and Supplementary Video 10), and in mTmG mice that had received PF4-mTmG lung transplants (Extended Data Fig. 2b). These extravascular cells were sessile during our imaging (up to 4 h) and contained large nuclei (Fig. 2c). Although they were comparatively large, these extravascular cells were on average one-third of the volume and approximately half of the diameter of intravascular megakaryocytes (Fig. 2d) and also smaller than resident megakaryocytes in the bone marrow and spleen (Extended Data Fig. 2c–e). Using image analysis, we detected around 2,000 PF4-tomato cells per cubic millimetre of lung tissue or more than 1 million cells per lung (Fig. 2e). The nuclear diameters of these cells were significantly larger than those of non-GFP$^+$ cells (Fig. 2f) and the nuclei had more complex shapes (Fig. 2g). We used a method of intravascular labelling before lung digestion[20] to determine the relative proportions of intravascular and extravascular megakaryocytes (Fig. 2i) and found that 85% of PF4-tomato events were extravascular and 15% intravascular (Fig. 2j).

To further characterize lung megakaryocytes, we sorted PF4-tomato$^+$ and CD41$^+$ cells from perfused and digested lungs and stained them with the megakaryocyte and platelet marker von Willebrand factor (vWF). The large, PF4-tomato$^+$ CD41$^+$ cells with complex nuclei also stained positive for vWF in a granular pattern, which is consistent with megakaryocytes (Fig. 2h). To avoid cell aggregation with PF4-tomato$^+$ platelets during flow cytometry staining, we prepared digested lungs from PF4-nTnG mice, in which GFP is targeted to the cell nucleus and thus does not stain anucleate platelets. We gated on nGFP$^+$ CD41$^+$

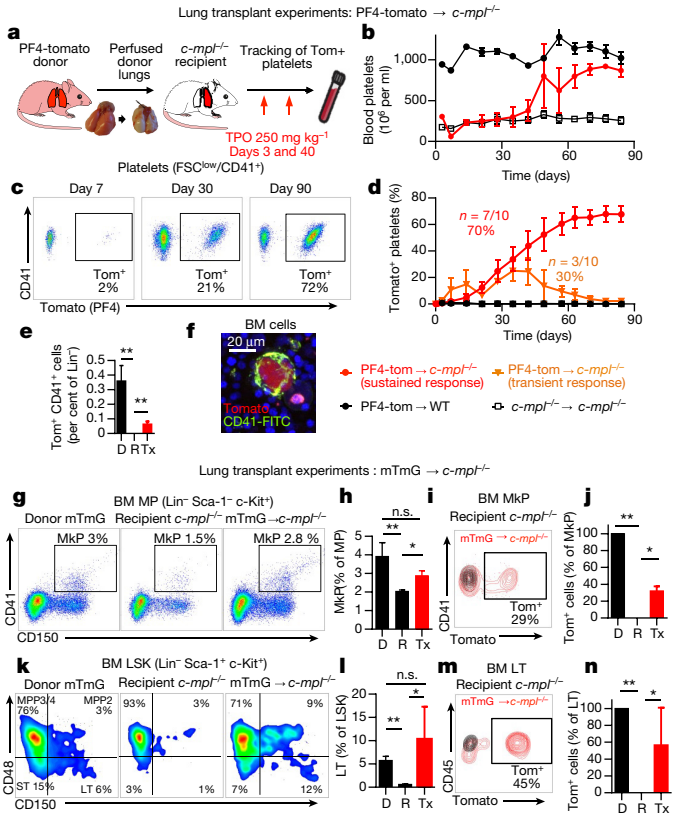


**Figure 3 | Lung-derived progenitors reconstitute platelet counts and haematopoietic stem cell deficiency in thrombocytopenic mice.** **a**–**f**, Transplantation of PF4-tomato lungs to *c-mpl*$^{-/-}$ mice. **a**, Experimental schema. **b**, Blood platelet counts ($n = 4$–6 mice per group). **c**, **d**, Percentage of donor-derived platelets analysed by counting tomato$^{+}$ events in the CD41$^{+}$ FSC$^{low}$ gate. **b**, **d**, Mean ± s.e.m. presented. **e**, **f**, Bone marrow cells from donor (PF4-tom), recipient (*c-mpl*$^{-/-}$) or transplanted mice with 10 months sustained donor-derived platelet production (Lung Tx) were analysed. **e**, FACS analysis of bone marrow cells reveals Tomato$^{+}$ cells (CD41$^{+}$ and CD41$^{-}$ populations). Percentage of lineage-negative bone marrow cells positive for Tomato and CD41. **f**, Representative immunofluorescence image of Tomato$^{+}$ cell (red) in the bone marrow of a transplanted mouse stained with anti-CD41 (green) and Syto60 nucleic acid stain (blue). **g**–**n**, Transplantation of mTmG lungs into *c-mpl*$^{-/-}$ mice. Bone marrow cells from donor (D, mTmG), recipient (R, *c-mpl*$^{-/-}$), or transplanted (Tx) mice with sustained donor-derived platelet production (3 months) were analysed. **g**, Representative FACS analysis of the myeloid progenitor compartment and the MkP population. **h**, Percentage of the MkP population within the myeloid progenitor compartment. **i**, **j**, Percentage of donor origin Tomato$^{+}$ cells in the MkP population. **k**, Representative FACS analysis of the LSK compartment showing MPP2, MPP3/4, ST-HSC and LT-HSC population frequencies within the LSK compartment. **l**, Percentage of the LT-HSC population within the LSK compartment. **m**, **n**, Percentage of donor origin Tomato$^{+}$ cells in the LT-HSC population. **h**, **j**, **l**, **n**, Mean ± s.d. are presented ($n = 2$–4 mice per group). Unpaired *t*-test: $^{**}P < 0.01$, $^{*}P < 0.05$; n.s., not significant.

events as the putative lung megakaryocyte pool (Fig. 2k and Extended Data Fig. 3a) and this population stained for the megakaryocyte and platelet-specific markers glycoprotein VI (GP VI) and the TPO receptor c-Mpl (Fig. 2k), but did not stain for markers of other lung resident cells, such as F4/80 for macrophages (Fig. 2k and Extended Data Fig. 3a–d) confirming that these lung-derived cells were megakaryocytes. The majority of the nGFP$^{+}$ cells in the lung were CD41$^{-}$ (Extended Data Fig. 3b), but both CD41$^{+}$ and CD41$^{-}$ cells co-stained for GPVI and c-Mpl, confirming their megakaryocyte lineage (Extended Data Fig. 3c). The nGFP$^{+}$ CD41$^{-}$ cells had a more immature profile with lower CD61 and CD42b expression, a smaller size and lower DNA content than the nGFP$^{+}$ CD41$^{+}$ cells (Extended Data Fig. 3e–i). Overall, lung megakaryocytes were more immature than bone marrow megakaryocytes (Extended Data Fig. 3j–m), but the total number of megakaryocytes in the lungs was comparable to that in the bone marrow (Fig. 2l, m). We also used RNA-sequencing (RNA-seq) to characterize lung and bone marrow megakaryocytes (nGFP$^{+}$ CD41$^{+}$ cells) in PF4-nTnG mice. We identified more than 700 genes that were expressed differentially in the lungs and bone marrow (Extended Data Fig. 4a and Supplementary Table 1); many megakaryocyte and platelet pathways were represented in both groups, but there was less expression of mature megakaryocyte markers in the lung group (Extended Data Fig. 4b, c), consistent with our profiling by immunostaining.

Lung 2PIVM indicated that only intravascular megakaryocytes released platelets. To test the function of extravascular megakaryocytes in the lungs, we used the orthotopic single-lung transplant model to adoptively transfer lung-resident cells. PF4-tomato donor lungs were extensively perfused and the left lungs were immediately transplanted into wild-type or *c-mpl*$^{-/-}$ thrombocytopenic recipient mice (Fig. 3a). These transplanted mice were injected with TPO at 3 and 40 days post-transplantation and bled weekly to track the number of platelets (Fig. 3a, b). Peripheral blood tomato$^{+}$ events after lung transplantation are, by definition, of donor lung origin. In wild-type recipients, we detected low-level (1–2% of total CD41$^{+}$ events) and transient production of tomato$^{+}$ events (Fig. 3d and Extended Data Fig. 5i). However, in the majority (70%) of *c-mpl*$^{-/-}$ recipients, we detected large and sustained (90 days) production of tomato$^{+}$ events (Fig. 3c, d and Extended Data Fig. 5c, d) that fully reconstituted platelet counts (Fig. 3b and Extended Data Fig. 5g, h). We observed the same response in two out of five *c-mpl*$^{-/-}$ recipients not treated with TPO after transplantation (Extended Data Fig. 5a, b, e, f). The tomato$^{+}$ CD41$^{+}$ events were also positive for CD42, GPVI and c-Mpl (Extended Data Fig. 6a, b) and expressed CD62P when stimulated with thrombin (Extended Data Fig. 6c–e), confirming that they were platelets.

In selected experiments, *c-mpl*$^{-/-}$ lung transplant recipients were followed for up to 10 months after transplantation. In these mice, we observed sustained production of tomato$^{+}$ platelets and sustained reconstitution of platelet counts (Extended Data Fig. 5j, k). Because platelet lifespan in mice is 3–5 days[21], the persistence of donor-origin platelets for more than 3 months suggested that the transplanted lungs contained a progenitor population capable of long-term reconstitution of mature megakaryocytes and platelets. Indeed, the fact that the extravascular megakaryocytes were smaller than the intravascular megakaryocytes in the lungs and the extravascular megakaryocytes in the bone marrow and spleen could point to the presence of megakaryocyte progenitors.

We imaged lungs 3 months after transplantation and confirmed the persistence of PF4-tomato cells (Extended Data Fig. 7a). We also detected the presence of tomato$^{+}$ CD41$^{+}$ cells in the bone marrow of *c-mpl*$^{-/-}$ mice that had received PF4-tomato lung transplants using flow cytometry (Fig. 3e) and immunofluorescence (Fig. 3f and Extended Data Fig. 7b). To test for lung megakaryocyte progenitors and to track donor cells in recipient mice, we transplanted mTmG lungs, in which all cells and platelets are tomato$^{+}$, into *c-mpl*$^{-/-}$ mice (Extended Data Fig. 7c–e). We next quantified the megakaryocyte progenitor (MkP) population in the bone marrow of *c-mpl*$^{-/-}$ mice transplanted with mTmG lungs by staining myeloid progenitors (Lin$^{-}$ Sca-1$^{-}$ c-Kit$^{+}$) for CD41 and CD150[22] (Fig. 3g). We found more myeloid progenitors and MkPs in the bone marrow of the lung transplant recipients than in *c-mpl*$^{-/-}$ bone marrow; the numbers in the transplant recipients were similar to the numbers of myeloid progenitors and MkPs normally found in the bone marrow of wild-type (mTmG) mice (Fig. 3h and Extended Data Fig. 7f, g). One-third of the MkPs in the bone marrow of *c-mpl*$^{-/-}$ mice transplanted with mTmG lungs expressed tomato (Fig. 3i, j).

We next tested whether the haematopoietic stem cell (HSC) deficiency characteristic of *c-mpl*$^{-/-}$ bone marrow[9] could be reversed by lung transplantation. We gated on the bone marrow LSK (Lin$^{-}$ Sca-1$^{+}$

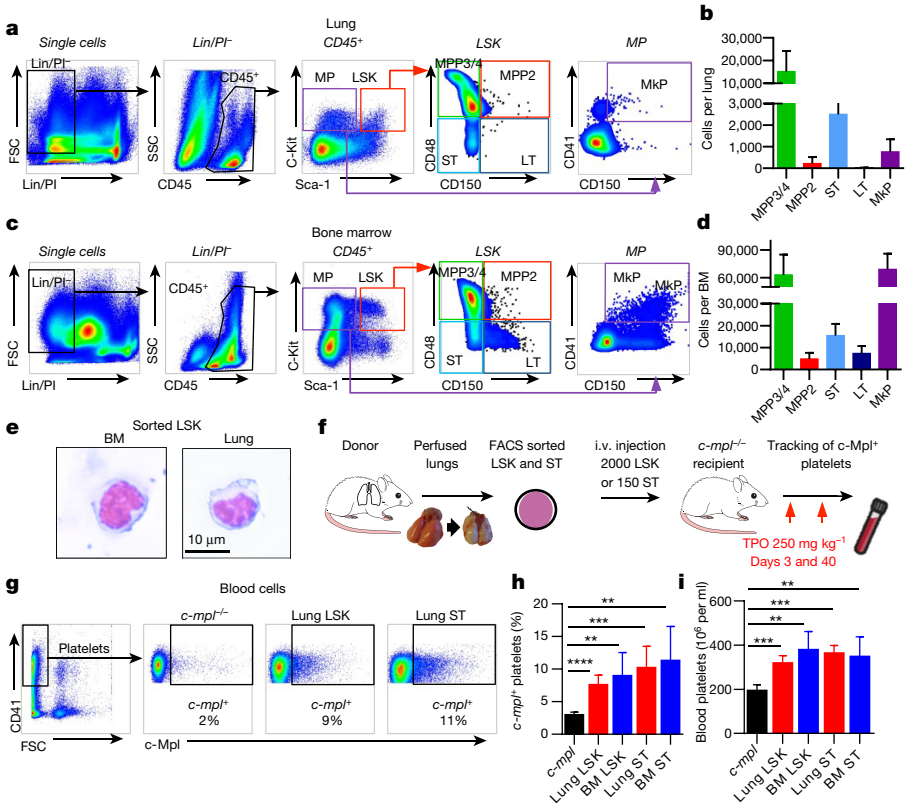


**Figure 4 | The lung contains haematopoietic progenitors, including megakaryocyte progenitors. a**, **c**, Representative lung (**a**) and bone marrow (**c**) FACS plots of haematopoietic progenitors within the LSK and myeloid progenitor compartments. **b**, **d**, Cell counts of haematopoietic progenitor (MPP2, MPP3/4, ST-HSC, LT-HSC, and MkP) populations in whole lungs ($n = 12$) (**b**) and bone marrow ($n = 5$) (legs, **d**). **e**, Representative image of Wright-Giemsa staining of LSK cells sorted from bone marrow or lung. **f**, Experimental schema. **g**, **h**, Percentage of donor-derived platelets analysed by FACS counting of c-Mpl$^+$ events in the CD41$^+$ FSC$^{small}$ gate. **i**, Blood platelet counts. **h**, **i**, Mean ± s.d. presented ($n = 4$–5 mice per group). Unpaired *t*-test: $^{**}P < 0.01$, $^{***}P < 0.001$, $^{****}P < 0.0001$.

c-Kit$^+$) population and probed for the following subsets: long-term HSCs (LT-HSCs; CD48$^-$ CD150$^+$), short-term HSCs (ST-HSCs; CD48$^-$ CD150$^-$), multipotent progenitor 2 (MPP2) cells (CD48$^+$ CD150$^+$), and MPP3/4 cells (CD48$^+$ CD150$^-$)[23] (Fig. 3k). Lung transplantation from TPO-competent (mTmG) donors reversed the LSK population deficiencies (Fig. 3l and Extended Data Fig. 7h–l). Lung–derived MkPs, LT-HSCs, ST-HSCs, MPP2s and MPP3/4s were also found in the bone marrow, spleen and recipient lungs (Fig. 3m, n and Extended Data Fig. 7n–p). A non-specific post-lung transplantation response was ruled out because transplantation of *c-mpl*$^{-/-}$ lungs into *c-mpl*$^{-/-}$ mice did not produce increased platelet counts (Fig. 3b) or alter the bone marrow composition (Extended Data Fig. 7m). Together, these results suggest that a haematopoietic progenitor population residing in the lungs can migrate to the bone marrow and reverse HSC defects and associated cytopenias.

We tested for haematopoietic progenitors in dispersed wild-type lungs using similar gating on live CD45$^+$ Lin$^-$ Sca-1$^+$ c-Kit$^+$ cells as in the bone marrow. We discovered that the lungs contain an array of haematopoietic progenitors, including ST-HSCs, MPP2s, MPP3/4s, myeloid progenitors and MkPs (Fig. 4a, b), which were morphologically indistinguishable from bone marrow LSK cells (Fig. 4e). These cells were present at lower numbers than in the bone marrow (Fig. 4c, d) and spleen (Extended Data Fig. 8a, b), except that there were more ST-HSCs in the lungs than in the spleen. These cells were extravascular, because they were not removed by perfusion and were not stained by intravascular CD45-APC antibodies (Extended Data Fig. 8c–h). To our knowledge, this is the first description of haematopoietic progenitor cells in the adult lungs, and we reasoned that these cells could be the source of the reconstituting effects of lung transplantation. To test this hypothesis, we isolated LSK and ST-HSCs from perfused wild-type lungs (and the bone marrow for comparison), injected these cells intravenously into *c-mpl*$^{-/-}$ recipients, and tested for the presence of c-Mpl$^+$ platelets in the peripheral blood (Fig. 4f). Injection of lung LSK cells and ST-HSCs increased peripheral c-Mpl$^+$ platelets and partially restored platelet counts, and injection of bone marrow cells had a similar effect (Fig. 4g–i). These results show that the adult lungs contain functional haematopoietic precursors capable of migration, bone marrow engraftment, and reconstitution of haematopoietic defects.

Finally, we tested whether lung haematopoietic progenitors are capable of multi-lineage bone marrow reconstitution. We transplanted lungs from mTmG donors to allow us to track mature lineages in the peripheral blood and bone marrow (Extended Data Fig. 7c), and detected sustained production of donor-derived (tomato$^+$ CD41$^-$) cells in the peripheral blood of the *c-mpl*$^{-/-}$ recipient mice (Extended Data Fig. 8i, j). The donor-derived cells included platelets (Extended Data Fig. 7d, e), neutrophils, and B and T cells (Extended Data Fig. 8k). Considering that there are no neutrophil, B cell or T cell defects in *c-mpl*$^{-/-}$ mice and therefore no impetus for donor-derived reconstitution, these results demonstrate an important contribution of the lungs to overall haematopoiesis.

Our results provide direct evidence that the lungs are a major site of platelet biogenesis, which involves a distinct mechanism of proplatelet release from intravascular megakaryocytes (of extrapulmonary origin) in the lung microcirculation (Extended Data Fig. 9a). These results open new lines of investigation to improve our approach to treating thrombocytopenia, which affects millions of patients worldwide and causes substantial morbidity and mortality. We propose that the lungs are an ideal bioreactor for the production of mature platelets from megakaryocytes, and could advance studies of the treatment of thrombocytopenia with cell-based therapies[16]. Beyond the mechanical forces that

promote proplatelet formation and extension, the lung may contain unique signalling partners for megakaryocytes that promote platelet release. Interactions between megakaryocytes and endothelial cells through glycoprotein 1b (GPIb)–vWF signalling have been shown to promote proplatelet formation *in vitro*[24]. Considering that vWF levels are particularly high in the pulmonary arteries[25], this pathway could finely regulate megakaryocytes for platelet production.

The lungs are a reservoir for resident megakaryocytes and haematopoietic progenitor cells (Extended Data Fig. 9b), which raises questions about the factors responsible for the homing of these cells into and out of the lungs, the function of these cells in the lung niche, and the roles of these cells in host defence[26]. Additionally, megakaryocytes are a rich source of cytokines and growth factors that have the potential to influence inflammatory or fibrotic lung diseases. Our RNA-seq analysis revealed that lung megakaryocytes were skewed towards an innate immunity function (Extended Data Fig. 4d–f and Supplementary Table 1), which may reflect the unique environment of the exposed lung versus the bone marrow. Indeed, we detected changes in the resident and circulating lung megakaryocyte populations in mice with bacterial pneumonia (Extended Data Fig. 4g–k). Our findings may also be applicable to the field of lung transplantation, in which post-transplantation chimaerism could affect acute and chronic allograft rejection. Our results add to the growing evidence that the lungs are a sophisticated organ that is capable of regeneration after major injury, are a major site of platelet production, and have untapped potential as a contributor to haematopoiesis.

**Online Content** Methods, along with any additional Extended Data display items and Source Data, are available in the online version of the paper; references unique to these sections appear only in the online paper.

**Received 24 April 2016; accepted 14 February 2017.**
**Published online 22 March 2017.**

1. Semple, J. W., Italiano, J. E., Jr & Freedman, J. Platelets and the immune continuum. *Nat. Rev. Immunol.* **11,** 264–274 (2011).
2. Versteeg, H. H., Heemskerk, J. W., Levi, M. & Reitsma, P. H. New fundamentals in hemostasis. *Physiol. Rev.* **93,** 327–358 (2013).
3. Machlus, K. R. & Italiano, J. E. Jr. The incredible journey: from megakaryocyte development to platelet formation. *J. Cell Biol.* **201,** 785–796 (2013).
4. Howell, W. H. & Donahue, D. D. The production of blood platelets in the lungs. *J. Exp. Med.* **65,** 177–203 (1937).
5. Levine, R. F. *et al.* Circulating megakaryocytes: delivery of large numbers of intact, mature megakaryocytes to the lungs. *Eur. J. Haematol.* **51,** 233–246 (1993).
6. Zucker-Franklin, D. & Philipp, C. S. Platelet production in the pulmonary capillary bed: new ultrastructural evidence for an old concept. *Am. J. Pathol.* **157,** 69–74 (2000).
7. Weyrich, A. S. & Zimmerman, G. A. Platelets in lung biology. *Annu. Rev. Physiol.* **75,** 569–591 (2013).
8. Looney, M. R. *et al.* Stabilized imaging of immune surveillance in the mouse lung. *Nat. Methods* **8,** 91–96 (2011).
9. Alexander, W. S., Roberts, A. W., Nicola, N. A., Li, R. & Metcalf, D. Deficiencies in progenitor cells of multiple hematopoietic lineages and defective megakaryocytopoiesis in mice lacking the thrombopoietic receptor c-Mpl. *Blood* **87,** 2162–2170 (1996).
10. Aschoff, L. Uber capillare Embolie von riesenkemhaltigen Zellen. *Arch Pathol Anat Phys* **134,** 11–14 (1893).
11. Kallinikos-Maniatis, A. Megakaryocytes and platelets in central venous and arterial blood. *Acta Haematol.* **42,** 330–335 (1969).
12. Tiedt, R., Schomber, T., Hao-Shen, H. & Skoda, R. C. Pf4-Cre transgenic mice allow the generation of lineage-restricted gene knockouts for studying megakaryocyte and platelet function *in vivo*. *Blood* **109,** 1503–1506 (2007).
13. Patel, S. R., Hartwig, J. H. & Italiano, J. E., Jr. The biogenesis of platelets from megakaryocyte proplatelets. *J. Clin. Invest.* **115,** 3348–3354 (2005).
14. Thon, J. N. *et al.* Cytoskeletal mechanics of proplatelet maturation and platelet release. *J. Cell Biol.* **191,** 861–874 (2010).
15. Trowbridge, E. A. *et al.* The origin of platelet count and volume. *Clin. Phys. Physiol. Meas.* **5,** 145–170 (1984).
16. Fuentes, R. *et al.* Infusion of mature megakaryocytes into mice yields functional platelets. *J. Clin. Invest.* **120,** 3917–3922 (2010).
17. Kaufman, R. M., Airo, R., Pollack, S. & Crosby, W. H. Circulating megakaryocytes and platelet release in the lung. *Blood* **26,** 720–731 (1965).
18. Sayah, D. M. *et al.* Neutrophil extracellular traps are pathogenic in primary graft dysfunction after lung transplantation. *Am. J. Respir. Crit. Care Med.* **191,** 455–463 (2015).
19. Junt, T. *et al.* Dynamic visualization of thrombopoiesis within bone marrow. *Science* **317,** 1767–1770 (2007).
20. Pereira, J. P., An, J., Xu, Y., Huang, Y. & Cyster, J. G. Cannabinoid receptor 2 mediates the retention of immature B cells in bone marrow sinusoids. *Nat. Immunol.* **10,** 403–411 (2009).
21. Liu, Z. J. *et al.* Expansion of the neonatal platelet mass is achieved via an extension of platelet lifespan. *Blood* **123,** 3381–3389 (2014).
22. Pronk, C. J. *et al.* Elucidation of the phenotypic, functional, and molecular topography of a myeloerythroid progenitor cell hierarchy. *Cell Stem Cell* **1,** 428–442 (2007).
23. Pietras, E. M. *et al.* Functionally distinct subsets of lineage-biased multipotent progenitors control blood production in normal and regenerative conditions. *Cell Stem Cell* **17,** 35–46 (2015).
24. Dunois-Lardé, C. *et al.* Exposure of human megakaryocytes to high shear rates accelerates platelet production. *Blood* **114,** 1875–1883 (2009).
25. Yamamoto, K., de Waard, V., Fearns, C. & Loskutoff, D. J. Tissue distribution and regulation of murine von Willebrand factor gene expression *in vivo*. *Blood* **92,** 2791–2801 (1998).
26. Haas, S. *et al.* Inflammation-induced emergency megakaryopoiesis driven by hematopoietic stem cell-like megakaryocyte progenitors. *Cell Stem Cell* **17,** 422–434 (2015).

**Supplementary Information** is available in the online version of the paper.

**Acknowledgements** We thank the UCSF BIDC for assistance with 2PIVM and 3D printing; A. Hérault, E. Verovskaya and S. Y. Zhang from the Passegué laboratory for assistance with hematopoietic progenitor isolation and transplantation; and D. Erle and the UCSF SABRE Functional Genomics Facility for assistance with the RNA-sequencing experiments. This work was supported in part by NIH grants HL092471 to E.P., HL107386 and HL130324 to M.R.L., the UCSF Nina Ireland Program in Lung Health (M.R.L.), and the UCSF Program for Breakthrough Biomedical Research (M.R.L.).

**Author Contributions** E.L. designed and conducted most of the experiments, analysed the data, and wrote the manuscript. G.O.-M. designed and conducted experiments and analysed the data. A.C. and B.M. conducted experiments and analysed data. F.L. performed the lung transplantation experiments. D.M.S., E.E.T., M.B.H. and T.D. assisted in designing and conducting experiments. S.R.C, M.F.K. and A.D.L. assisted in designing experiments and provided editorial support on the manuscript. E.P. assisted in designing experiments, provided technical expertise with haematopoietic progenitor analyses, and provided editorial support on the manuscript. M.R.L. designed the experiments, conducted experiments, analysed data, and wrote the manuscript.

**Author Information** Reprints and permissions information is available at www.nature.com/reprints. The authors declare no competing financial interests. Readers are welcome to comment on the online version of the paper. Publisher's note: Springer Nature remains neutral with regard to jurisdictional claims in published maps and institutional affiliations. Correspondence and requests for materials should be addressed to M.R.L. (mark.looney@ucsf.edu).

**Reviewer Information** *Nature* thanks F. Ginhoux, S. Morrison, G. Zimmerman and the other anonymous reviewer(s) for their contribution to the peer review of this work.

## METHODS

**Mice.** Mice were housed and bred under specific pathogen-free conditions at the University of California, San Francisco (UCSF) Laboratory Animal Research Center and all experiments conformed to ethical principles and guidelines approved by the UCSF Institutional Animal Care and Use Committee. Male and female mice between 8 and 12 weeks of age were used for experiments. C57BL/6, PF4-Cre, Rosa26-LSL-tdTomato, mTmG, nTnG and *Ptprc*$^{a}$ *Pepc*$^{b}$ BoyJ mice were purchased from Jackson Laboratories. To track platelets or megakaryocytes, PF4-Cre expressing mice were crossed with Rosa26-LSL-tdTomato, mTmG or nTnG reporter strains, in which the fluorophore of PF4-expressing cells (tdTomato or GFP) is localized to the cytoplasm, the cell membrane, or the nucleus, respectively. *c-mpl*$^{-/-}$ mice (C57BL/6 background) were obtained from a Material Transfer Agreement from Genentech.

**Lung intravital imaging.** We used 2PIVM to observe megakaryocyte and platelet production in real time in mouse lungs. A modified version[27] of the previously published method of stabilized lung imaging was used[8]. Mice were anaesthetized with ketamine and xylazine and secured with tape to a custom heated microscope stage. A small tracheal cannula was inserted, sutured into place, and attached to a MiniVent mouse ventilator (Harvard Apparatus). Mice were ventilated with a tidal volume of 10 μl compressed air (21% $O_2$) per gram of mouse weight, a respiratory rate of 130–140 breaths per minute, and a positive-end expiratory pressure of 2–3 cm $H_2O$. Isoflurane was delivered continuously to maintain anaesthesia and mice were injected with 300 μl of 0.9% saline solution intraperitoneally every hour. The mice were placed in the right lateral decubitus position and a small surgical incision was made to expose the rib cage. A second incision was then made into the intercostal space between ribs 4 and 5, through the parietal pleura, to expose the surface of the left lung lobe. A flanged thoracic window with an 8-mm coverslip was then inserted between the two ribs and secured to the stage using a set of two optical posts and a 90° angle post clamp (Thor Labs)[27,28]. We applied 20–25 mm Hg of suction (Amvex Corporation) to gently immobilize the lung. The two-photon microscope objective was then lowered into place over the thoracic window. In selected experiments, to permit identification of the lung vasculature, FITC dextran (50 μl of 25 mg/ml; Life Technologies) was injected intravenously into the tail vein before imaging.

**Spleen and liver intravital imaging.** Mice were anaesthetized and ventilated as noted above. To expose the spleen, a skin incision was made in the left flank. An incision was made along the costal margin to expose and externalize the liver. The same window as was used for lung imaging was used to facilitate imaging of the spleen and liver. The mouse was placed on a 37 °C temperature-controlled heated stage for the duration of the imaging and saline solution was administered intraperitoneally every hour.

**Bone marrow intravital imaging.** Mice were anaesthetized with an initial dose of ketamine and xylazine and anaesthesia was maintained with isoflurane delivered through a nose cone. Hair and the underlying subcutaneous tissue were removed to expose the calvarium. The periosteum was removed using a microsurgical knife. To stabilize the skull, we 3D printed an apparatus that was fixed to the mouse skull with Vetbond and attached to the heated stage below. The microscope objective was then lowered into a 5-mm bevelled hole filled with saline.

**Two-photon microscopy.** Intravital imaging was performed using a Nikon A1R Multi-photon microscope equipped with a Mai Tai DeepSee IR Laser (Spectra Physics) (UCSF BIDC). The MaiTai laser was tuned to 920 nm for simultaneous excitation of GFP or FITC and tdTomato. Emitted light was detected using a 25× water lens (Nikon) with green (500–550 nm) and red (570–620 nm) filters. Images were captured with a high-resolution galvano scanner (1 frame per second, 512 × 512 pixels). The microscope was controlled using NIS Element AR software (4.50). We captured a 1,052 μm × 1,578 μm $x$–$y$ surface area (1.66 $mm^2$) and $z$-stack images were acquired with $z$-depths of 5 μm (total of 40 μm $z$-depth). We captured a complete image every 1 min for 120 min.

**Image analysis.** Images were analysed using Imaris 7.6.1 (Bitplane) or NIS-Element (Nikon) software (UCSF BIDC). Surface analysis was performed to quantify and characterize the volume, diameter, or circularity of resident and circulating megakaryocytes or platelets. Megakaryocytes or megakaryocyte fragments were defined as $PF4^+$ events with a diameter >15 μm. Platelets were defined as $PF4^+$ events with a diameter between 0.5 and 5 μm. To calculate the number of platelets released by each megakaryocyte observed, the ratio of the megakaryocyte to platelet volumes was calculated for each of the 35 fragmenting megakaryocytes or proplatelets observed during lung imaging. Megakaryocytes were divided into three groups according to the number of platelets that can be produced by one megakaryocyte: small (<500 platelets, $n = 18$), medium (500–1,000 platelets, $n = 7$) and large (>1,000 platelets, $n = 10$).

**Quantifying platelet production in the lung (see variables in Extended Data Table 1).** For each movie (~2 h), the megakaryocytes observed to be undergoing fragmentation in the lung ($LungMK_{frag}$) were quantified: $LungMK_{frag}$ per hour = ($LungMK_{frag}$)/(Acquisition time in min) × 60. The number of platelets released by each megakaryocyte undergoing fragmentation in the lung was calculated using the volume ratio of the megakaryocyte volume to the average platelet volume: $N_{Plat/MK} = Volume_{MK}/Volume_{Plat}$. The number of platelets produced in the lung was then calculated: $Lung_{Platelets}$ per hour = $LungMK_{frag}$ per hour × $N_{Plat/MK}$ × Lung fraction, where the lung fraction is the ratio of the mouse total lung volume[29] to the observed lung volume: Lung fraction = $Volume_{lung}/Volume_{observed}$. Finally, we estimated the contribution of the lung to overall thrombopoiesis: % lung platelet production = (Lung platelets per hour × 24)/(Total Platelets per day) × 100.

The total number of platelets produced per day was calculated according to the number of circulating platelets in the mouse blood divided by the life span of platelets, and takes into account the fact that one-third of the produced platelets are sequestered by the spleen: total platelets per day = ($Plat_{Blood}(1 + Plat_{Spleen})$)/($Life_{Plat}$). In selected experiments, mice were treated with recombinant human thrombopoietin (rhTPO, Genentech) intraperitoneally (250 mg/kg), 5 days before lung imaging.

**Lung, bone marrow, spleen and blood single-cell preparation for flow cytometry or cell sorting.** *Lung digestion*. For lung HSC or megakaryocyte cell sorting, lungs were perfused before removal and digestion. Lungs were placed in 2 ml PBS with 5 μl/ml DnaseI (Roche) and 0.5 mg/ml LiberaseTM (Roche), minced with scissors in 15-ml tubes, and digested for 30 min at 37 °C before filtration through a 100-μm cell strainer and red blood cell lysis. Samples were then filtered through a 40-μm filter and resuspended for subsequent FACS staining. For experiments in which vascular localization was tested, mice were injected intravenously with CD41–APC (eBioscience) or CD45-APC (eBioscience) 5 min before lung collection.

*Bone marrow isolation.* Tibias and femurs from both legs were removed from mice following euthanasia. Bone marrow cells were flushed with PBS with 5 mM EDTA before filtration through a 70-μm cell strainer and red blood cell lysis.

*Spleen isolation.* The spleen was removed and pressed with the end of a plunger from a 1-ml syringe into 1-ml PBS with 5mM EDTA before filtration through a 70-μm cell strainer and red blood cell lysis.

**Flow cytometry and cell sorting.** For surface staining, cells or platelets were incubated with anti-Fc receptor antibodies (clone 2.4G2) and stained with antibodies in Hanks buffered salt solution (HBSS) with 2% fetal calf serum and 5 mM EDTA for 30 min.

Antibody clones used: CD41-APC (MWReg30, eBioscience), CD41-FITC (MWReg30, BD), CD41-BV421 (MWReg30, BioLegend), CD41-BV570 (MWReg30, BioLegend), c-mpl-Biotin (AMM2, IBL), streptavidin PE-Cy7 (BD), GPVI-FITC (JAQ1, emfret), F4/80-PB (CI:A3-1, BioLegend), CD45-APC (30F11, BioLegend), CD42d-APC (1C2, eBioscience), CD62P-APC (Psel. KO2.3, eBioscience). HSCs were stained with rat unconjugated Lin antibodies Gr-1 (RB6-8C5), Mac1 (M1/70), B220 (RA3-6B2), CD5 (53-7.3), CD4 (GK1.5), CD8 (53-6.7) (eBioscience), Ter-119 (BD), CD3 (17A2, BioLegend), goat anti-rat-PE-Cy5 (Invitrogen), c-Kit-APC-eFluor780 (2B8, eBioscience), Sca-1-PB (D7, BioLegend), CD48-APC (HM48-1, BioLegend), CD150-PE-Cy7 (TC15-12F12.2, BioLegend) and CD45.2-FITC (104, eBioscience). HSC and progenitor populations were defined as follows: myeloid progenitor ($Lin^-$ $CD45^+$ $Sca\text{-}1^-$ $c\text{-}Kit^+$), megakaryocyte progenitor ($CD150^+$ $CD41^+$), LSK compartment ($Lin^-$ $CD45^+$ $Sca\text{-}1^+$ $c\text{-}Kit^+$), MPP2 (LSK $CD48^+$ $CD150^+$), MPP3/4 (LSK $CD48^+$ $CD150^-$), ST-HSC (LSK $CD48^-$ $CD150^-$) and LT-HSC (LSK $CD48^-$ $CD150^+$). Mature blood cells were stained with CD19-PB (6D5, BioLegend), Gr-1 APC-Cy7 (RB6-8C5, eBioscience), CD3-PerCP710 (17A2, eBioscience), and CD11b-APC (M1/70, BD). For sorting HSCs, a $c\text{-}kit^+$ cell enrichment step was done before staining the cells using c-kit antibody-conjugated magnetic beads and MACS separation columns (Miltenyi Biotec). Stained cells were re-suspended for final analysis in Hanks buffered salt solution (HBSS) with 2% serum (FCS) and 1 μg/ml propidium iodide for dead cell exclusion. Samples were analysed on a LSRII flow cytometer (BD Biosciences) and cell sorting was performed using a BD FACS Aria II (BD Biosciences) in the UCSF Flow Cytometry Core. Analysis of flow cytometry data was performed using Flowjo (Treestar)

**Lung perfusion.** Lungs were perfused before lung transplant experiments, FACS, or cell analysis. Mice were anaesthetized with an intraperitoneal injection of ketamine (50 mg/kg) and xylazine (10 mg/kg). A 20-gauge angiocath was inserted into the trachea and connected to a ventilator. Through a midline abdominal incision the diaphragm was incised circumferentially and 0.1 ml heparin was injected directly into the inferior vena cava. A thoracotomy was performed to expose the heart and lungs. Cold PBS (5 ml) with 0.1 ml heparin solution was perfused directly into the right ventricle using a 27-gauge needle. The trachea was then tied and the heart–lung block removed and placed in a small tube containing PBS. In selected experiments, we also performed retrograde lung perfusion by instilling 5 ml cold PBS with 0.1 ml heparin solution into the left atrium.

**Lung transplant experiments.** Left lung transplants in mice were performed as previously described[18]. Lungs from PF4-tomato or mTmG donor mice were perfused and the left lung was immediately transplanted into C57BL/6 wild-type or *c-mpl*$^{-/-}$ recipients. Selected *c-mpl*$^{-/-}$ recipients received recombinant human thrombopoietin (rhTPO, Genentech) intraperitoneally (250 mg/kg) on days 3 and 40 after transplantation. Blood was collected from the submandibular vein every week to count blood platelets, donor-derived platelets (tomato$^{+}$ platelets) and donor-derived mature blood cells. The transplanted mice were analysed for 3 months and then euthanized for bone marrow, blood, and lung removal and analysis. In selected experiments, mice were allowed to survive for 10 months after transplantation before analysis. For 2PIVM after lung transplantation, a perfused mTmG lung was transplanted into a PF4-mTmG recipient or vice versa. The transplanted lung was imaged immediately after transplantation.

**Blood collection and platelet counting.** For whole blood analysis, blood was withdrawn from the submandibular vein for survival bleeding or by cardiac puncture in terminal experiments. Blood was collected into either acid citrate dextrose (Sigma-Aldrich) for flow cytometry analysis or EDTA tubes (BD microtainer) for platelet counting. Platelet counts in the peripheral blood were measured with a Hemavet 950 FS complete blood counting instrument (Drew Scientific) and confirmed using manual platelet counts.

**Cell immunofluorescence.** *Lung megakaryocytes.* Nucleated cells that were double-positive for tomato and CD41 were sorted from digested lung tissue and cytospin slides were prepared. The cells were fixed with PFA 4% and permeabilized with 0.5% Triton. After saturation with PBS/BSA 3%, cells were stained overnight at 4 °C with sheep anti-vWF antibody (Abcam) and 1 h with anti-Sheep AlexaFluor488 antibody (Invitrogen). Slides were mounted with DAPI mounting medium (Molecular Probes) and analysed on a Nikon TI-E high-throughput epifluorescence microscope (UCSF Nikon Center).

*Bone marrow cells after lung transplants.* Bone marrow cells were isolated (see single-cell preparation methods) and resuspended in 1 ml PBS-EDTA 5 mM. Two-hundred and fifty microlitres of the suspension was stained for 20 min at room temperature in the dark with 1 μm Syto60 (cell-permeant nucleic acid stain) and anti CD41-FITC (1 μl). Cells were washed, resuspended in PBS, and seeded in a 6-well plate for immediate imaging on a Nikon A1R Multi-photon microscope (UCSF BIDC). Cells were excited with a 920-nm laser for simultaneous excitation of FITC (green), tdTomato (red) and Syto60 nucleic acid stain (FarRed).

**Platelet activation assay.** To determine whether the tomato$^{+}$ CD41$^{+}$ events detected in the peripheral blood after lung transplantation were bona fide platelets, we stimulated whole blood with thrombin (10 nM) to induce the expression of P-selectin (RB40.34, BD)[30], which was measured by flow cytometric analysis and compared to platelets from PF4-tomato mice.

**MRSA infection.** We used the SF8300 strain of MRSA (methicillin-resistant *Staphylococcus aureus*, obtained from C. Chambers at UCSF), which is a minimally passaged USA300 clinical strain representative of the epidemic clone USA300-0114. Stock solutions of SF8300 at the mid-logarithmic growth phase ($10^{10}$ CFU/ml) were aliquoted and frozen at −80 °C using standard techniques. On the day of the experiment, a vial of SF8300 was thawed and diluted with PBS to the concentration needed ($5 \times 10^{7}$ CFU per mouse in 50 μl) for direct tracheal instillation into anaesthetized PF4-nTnG mice. Lungs were harvested 24 h after inoculation for single-cell preparation and flow cytometry. To test for vascular localization, mice were injected intravenously with CD41–APC (eBioscience) 5 min before lung collection and CD41-FITC staining.

**RNA-seq analysis.** For RNA-seq experiments, we used PF4-nTnG mice and sorted PF4$^{+}$ CD41$^{+}$ cells from lung and bone marrow prepared for single-cell suspension and flow cytometry analysis. For each experiment, tissue from four mice was pooled and cells were sorted directly into lysis buffer. Total mRNA was isolated from between $1 \times 10^{4}$ and $4 \times 10^{5}$ purified cells using a Dynabeads mRNA DIRECT kit (Ambion-Life Technologies). Three independent replicates were used for each population. An mRNA library was prepared by the UCSF SABRE Functional Genomics Facility using low input Nugen Ovation plus Nextera kit (<100 ng RNA) and sequencing was performed using a single-end 50-bp RNA-seq Illumina TruSeq Stranded PolyA library kit and an Illumina HiSeq 4000 machine. Sequencing yielded ∼432 million reads in total with an average read depth of 72 million reads per sample. Reads were then aligned to the mouse genome (aligner: STAR_2.4.2a aligner, alignment genome: Ensembl Mouse GRCm38.78) and genes that mapped uniquely to known mRNAs were used to assess differential expression between lung and bone marrow groups. Differential expression testing was carried out using DESeq2 v1.14.0.

Using a log ratio test and fold-change cutoffs (false discovery rate (FDR) <0.05), we found 705 genes that were differentially expressed: 543 were upregulated in lung megakaryocytes and 162 in bone marrow megakaryocytes. Functional pathways representative of each gene signature were analysed for enrichment in gene categories from the Gene Ontology Biological Processes (GO-BP) database (Gene Ontology Consortium) using DAVID Bioinformatics Resources. For gene signatures and each GO category, the significance of the number of overlapping genes in the two sets was calculated using a Fisher's exact test performed by the DAVID software. The *P* value resulting from this test reflects the probability of obtaining the observed overlap or greater by chance. GO-BP categories with at least three genes and $P < 0.001$ were identified.

**Statistical analysis.** For surface analysis, minimum-to-maximum boxplots are shown: the line in the middle of the box is plotted at the median, the box extends from the 25th to the 75th percentile and the whiskers go down to the smallest value and up to the largest. The + indicates the mean. Other results plotted as histograms are reported as mean ± s.d. and were analysed by *t*-test, and multi-group comparisons were performed using a one-way ANOVA test and Bonferroni post-hoc test (GraphPad PRISM version 5.0; GraphPad Software Inc.). In all cases where statistical significance is provided, variance was not statistically different between groups. Sample sizes were chosen on the basis of previous experience in the laboratory with respect to inherent variability in intravital imaging, lung transplantation, and cellular transplantation experiments. There is a 10% surgical failure rate with the mouse orthotopic lung transplantation surgery, and it was pre-established that these mice would be excluded from the analysis. Animals within each cohort were randomly assigned to treatment groups. Blinded analysis was not performed in these studies. *P* values of less than or equal to 0.05 were considered to be statistically significant, indicated by asterisks in figures, unless otherwise noted.

**Data availability.** The RNA-seq data that support the findings of this study have been deposited in the NIH SRA database with the accession code SRP097794.


27. Headley, M. B. *et al.* Visualization of immediate immune responses to pioneer metastatic cells in the lung. *Nature* **531,** 513–517 (2016).
28. Ortiz-Muñoz, G. *et al.* Aspirin-triggered 15-epi-lipoxin A4 regulates neutrophil-platelet aggregation and attenuates acute lung injury in mice. *Blood* **124,** 2625–2634 (2014).
29. Canals, M., Olivares, R. & Rosenmann, M. A radiographic method to estimate lung volume and its use in small mammals. *Biol. Res.* **38,** 41–47 (2005).
30. Cornelissen, I. *et al.* Roles and interactions among protease-activated receptors and P2ry12 in hemostasis and thrombosis. *Proc. Natl Acad. Sci. USA* **107,** 18605–18610 (2010).

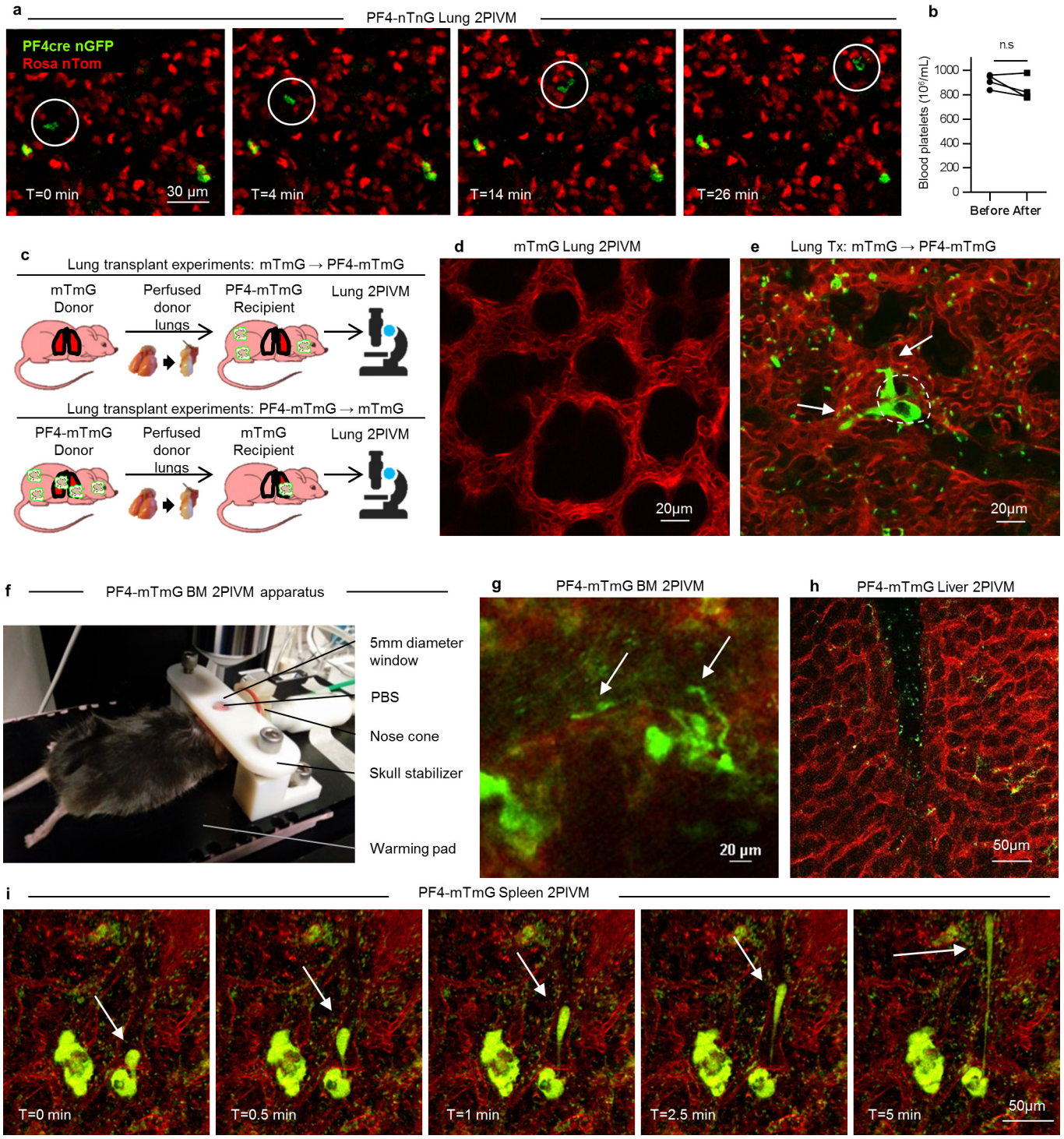


**Extended Data Figure 1 | Megakaryocytes and proplatelets observed in lung circulation are from an extrapulmonary source. a**, Lung 2PIVM of a PF4-nTnG mouse (nuclear GFP). The presence of the mobile GFP$^+$ nucleated cells (circled) indicates the presence of a nucleus in circulating megakaryocytes. **b**, Platelet counts in the blood before and after imaging. n.s., not significant ($n = 3$). **c**, Experimental schema of transplantation of lungs from mTmG mouse (perfused donor lung) to PF4-mTmG (recipient) mouse and vice-versa followed by 2PIVM. **d**, 2PIVM of a mTmG mouse lung showing no GFP signal. **e**, 2PIVM of an mTmG mouse lung transplanted into a PF4-mTmG recipient mouse showing GFP$^+$ cells from recipient and platelet production in the lung. **f**, Bone marrow 2PIVM apparatus. **g**, Representative image of proplatelet release in bone marrow (BM) sinusoids (arrows). **h**, 2PIVM of PF4-mTmG mouse liver. Small platelets (GFP, green) were seen in the circulation but neither resident nor circulating megakaryocytes or proplatelets were observed. **i**, 2PIVM of PF4-mTmG mouse spleen. Sequential images show resident megakaryocytes (GFP, green) releasing proplatelets (arrows) in the spleen vasculature (in red).

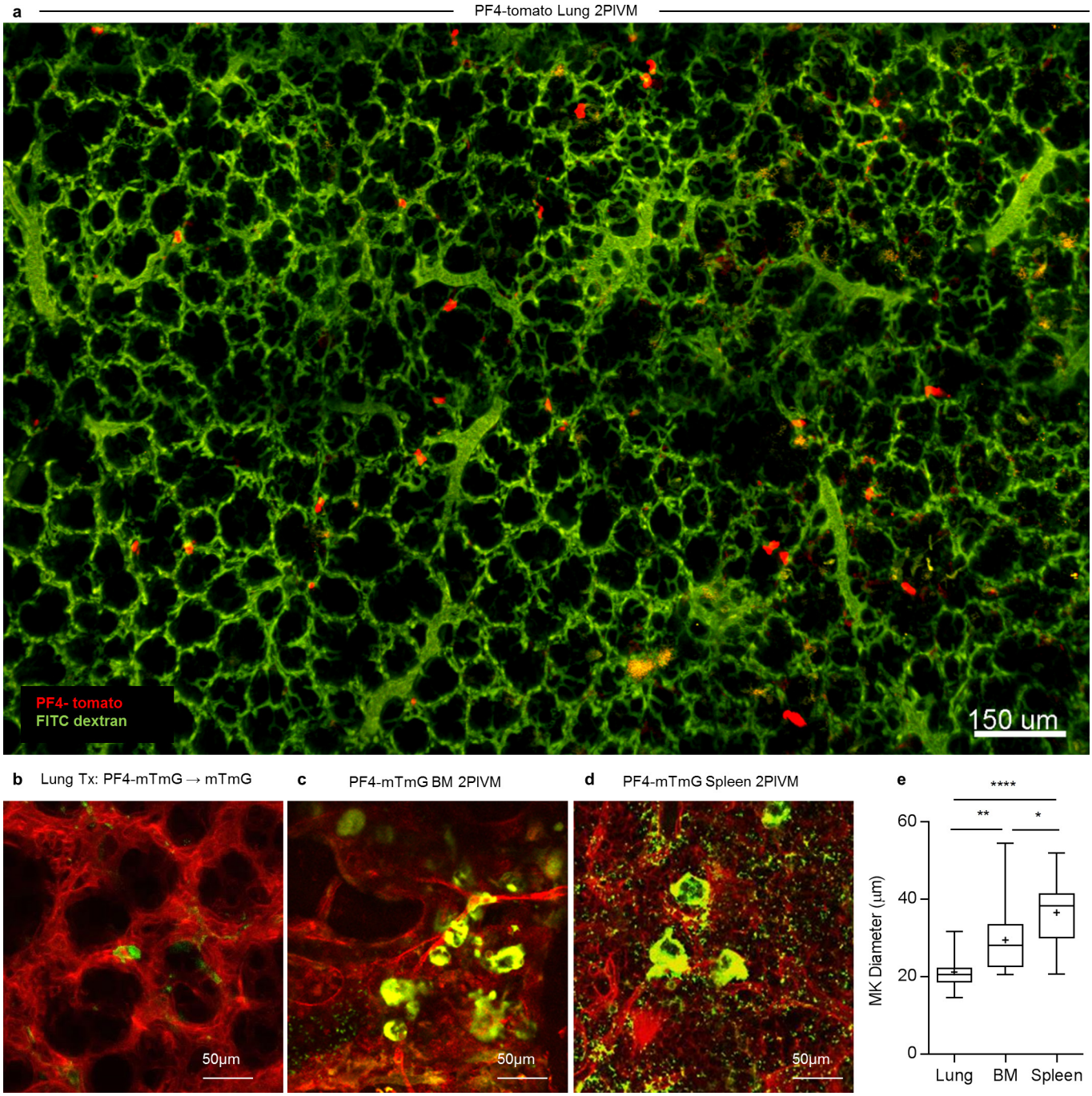


**Extended Data Figure 2 | Resident megakaryocytes in the lungs and other organs. a**, Survey of PF4-tomato mouse lung visualized by 2PIVM. PF4-tomato-expressing cells (red) are found in high numbers in the lungs. Lung vasculature is labelled by intravascular injection of FITC dextran (green). A total area of 2.49 $mm^2$ (1.6 mm × 1.6 mm) was imaged. **b**, Resident (static) $GFP^+$ cells are found in a PF4-mTmG lungtransplanted into an mTmG mouse. **c**, **d**, 2PIVM images of bone marrow (**c**) and spleen (**d**) from PF4-mTmG mice. Many large megakaryocytes (GFP, green) are found in the bone marrow and spleen. **e**, Size characterization of resident (static) $GFP^+$ cells by image analysis of PF4-mTmG lungs ($n = 16$), bone marrow ($n = 12$), and spleen ($n = 16$). Minimum-to-maximum boxplots are shown: the line in the middle of the box is plotted at the median, the box extends from the 25th to 75th percentiles and the whiskers range from the smallest to the largest values. The + indicates the mean.

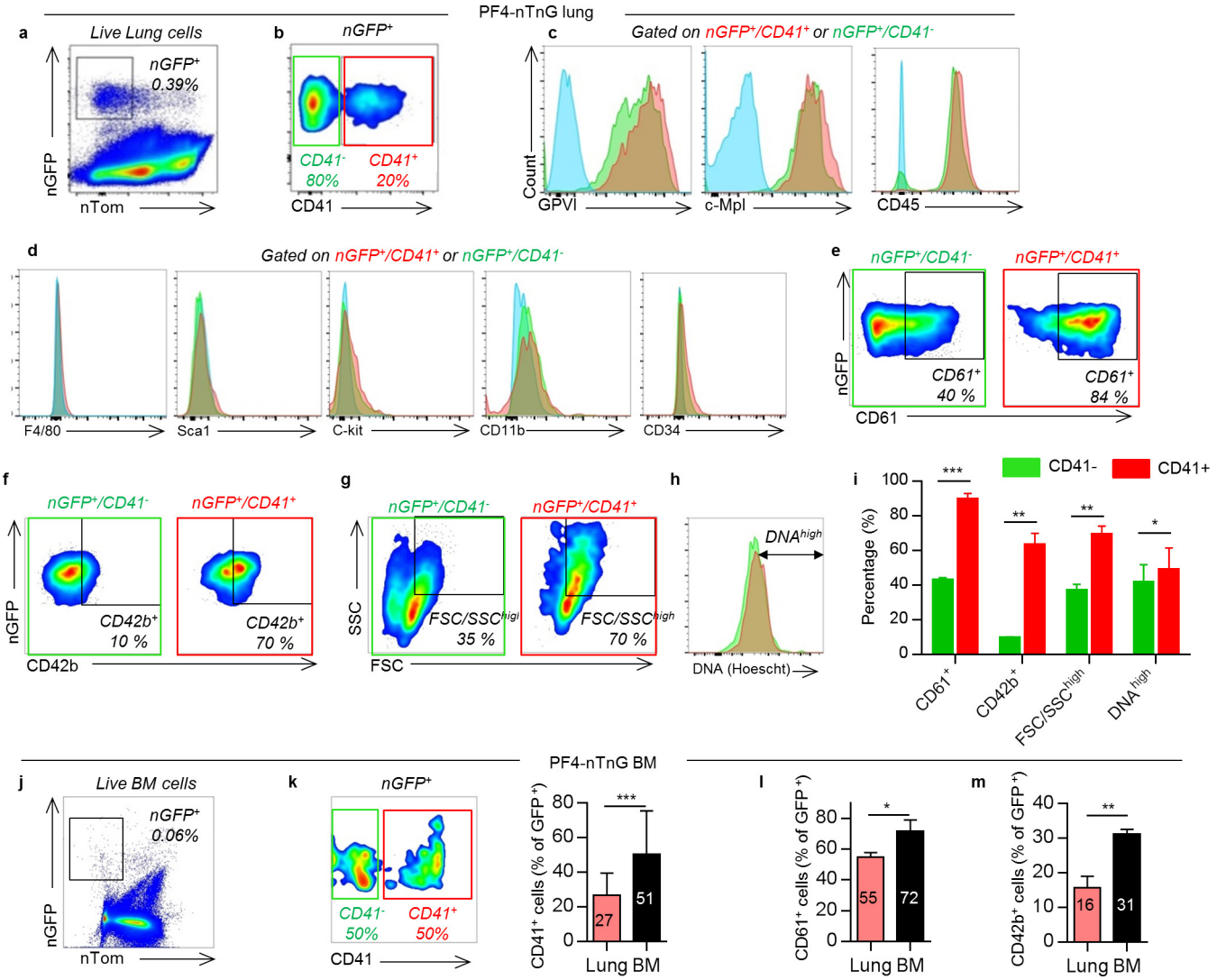


**Extended Data Figure 3 | Surface expression of lung megakaryocytes compared to bone marrow megakaryocytes. a**, Flow cytometric analysis of nGFP$^+$ cells from PF4-nTnG lungs. **b**, CD41 expression defines two populations of megakaryocytes: CD41$^+$ (red) and CD41$^-$ (green). **c**, Positive surface expression of GPVI, c-Mpl and CD45 was detected in both populations. Unstained cells are plotted in blue. **d**, Surface expression of F4/80, CD34, CD11b, Sca-1 and c-Kit was not detected. **e**–**i**, The CD41$^+$ population has a higher percentage of CD61$^+$ cells (**e**), CD42b$^+$ cells (**f**) and larger cells (**g**) and had higher DNA content (**h**), as summarized in **i** ($n = 3$). **j**, Flow cytometric analysis of nGFP$^+$ cells from PF4-nTnG bone marrow. **k**–**m**, Compared to the lungs, the bone marrow nGFP$^+$ population has a higher percentage of CD41$^+$ cells ($n = 21$–$23$) (**k**), CD61$^+$ cells ($n = 3$) (**l**), and CD42b$^+$ cells ($n = 3$) (**m**). Data are representative of three or more replicates. Mean ± s.d. are presented. Unpaired *t*-test: $^*P < 0.05$, $^{**}P < 0.01$, $^{***}P < 0.001$.

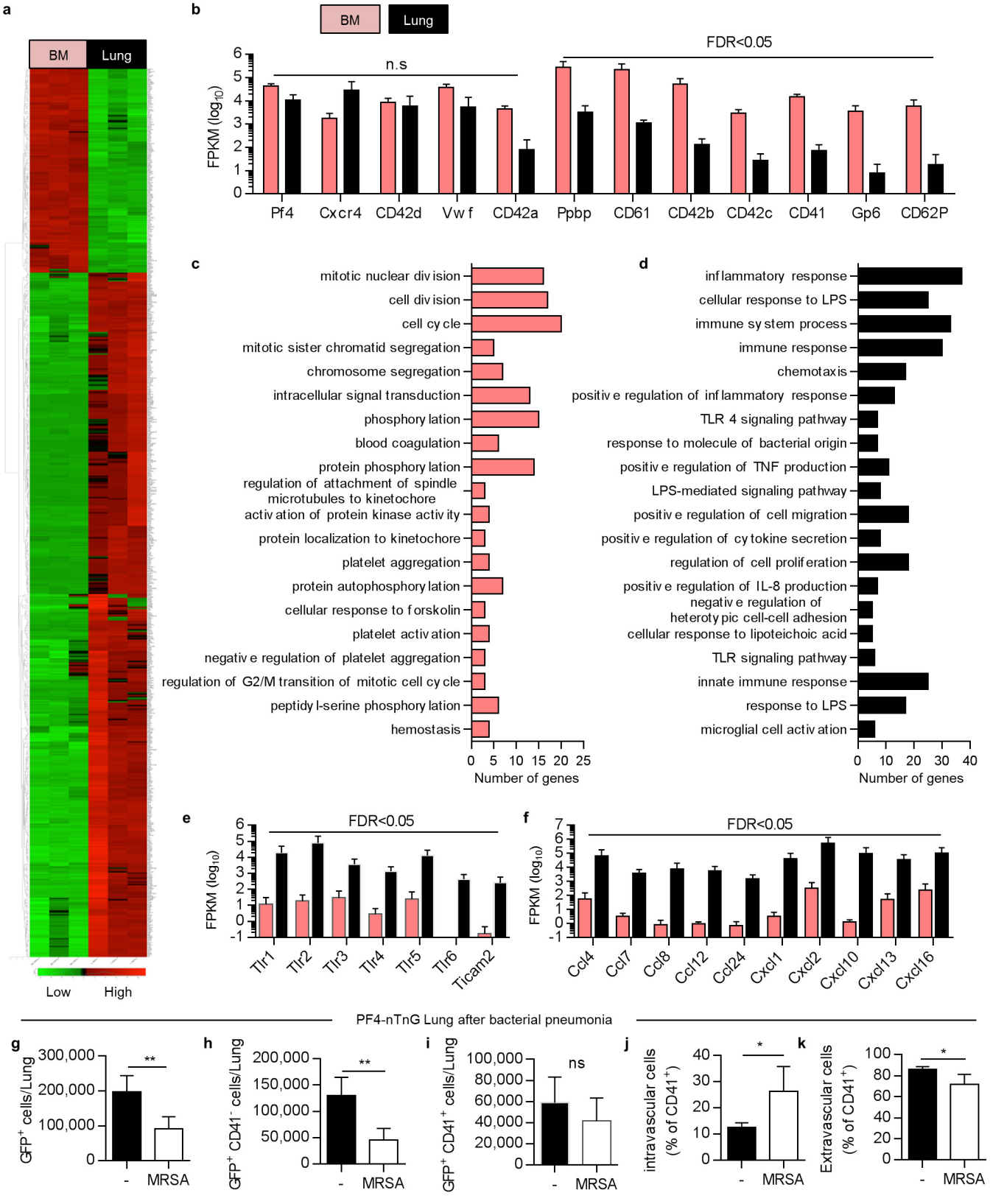


**Extended Data Figure 4** | See next page for caption.

**Extended Data Figure 4 | Gene expression analysis of lung versus bone marrow megakaryocytes and bacterial pneumonia experiment reveal an immature profile and a potential role in immunity for lung megakaryocytes.** Megakaryocytes (nGFP$^+$ CD41$^+$) were sorted from PF4-nTnG lungs and bone marrow followed by mRNA isolation and sequencing. **a**, Relative mRNA expression is shown on a scale from low (green) to high (red). Three independent experiments (four mice each) were used for statistical analysis. Heatmap of all significantly differentially expressed genes (FDR $<0.05$). **b**, Read counts for megakaryocyte-related genes. These genes are found in both lung and bone marrow megakaryocytes, but some are underrepresented in lung megakaryocytes. **c**, **d**, Analysis of gene ontology biological processes related to genes that are downregulated (**c**) or upregulated (**d**) in lung megakaryocytes. The top 20 biological processes are shown. The vertical axis represents gene ontology categories, and the horizontal axis indicates the number of genes in each ontology category. **e**, **f**, Read counts for TLR gene pathways (**e**) and chemokines (**f**) that were overexpressed in lung megakaryocytes. FPKM, fragments per kilobase of exon per million fragments mapped. **g**–**k**, Lung megakaryocytes and progenitor populations are altered during infection. Flow cytometric analysis of nGFP$^+$ cells from PF4-nTnG lungs 24 h after intratracheal administration of *S. aureus* (MRSA, $5 \times 10^7$ colony-forming units (c.f.u.)). CD41–APC was injected intravenously before lung digestion and staining with CD41–FITC. The number of cells in normal or infected lungs are shown for all nGFP$^+$ cells (**g**), less mature cells (nGFP$^+$ CD41$^-$; **h**), and mature cells (nGFP$^+$ CD41$^+$; **i**). **j**, **k**, Percentage of intravascular megakaryocytes (**j**) and extravascular megakaryocytes (**k**) in the mature population (nGFP$^+$ CD41$^+$). $n = 4$–6 mice per group.

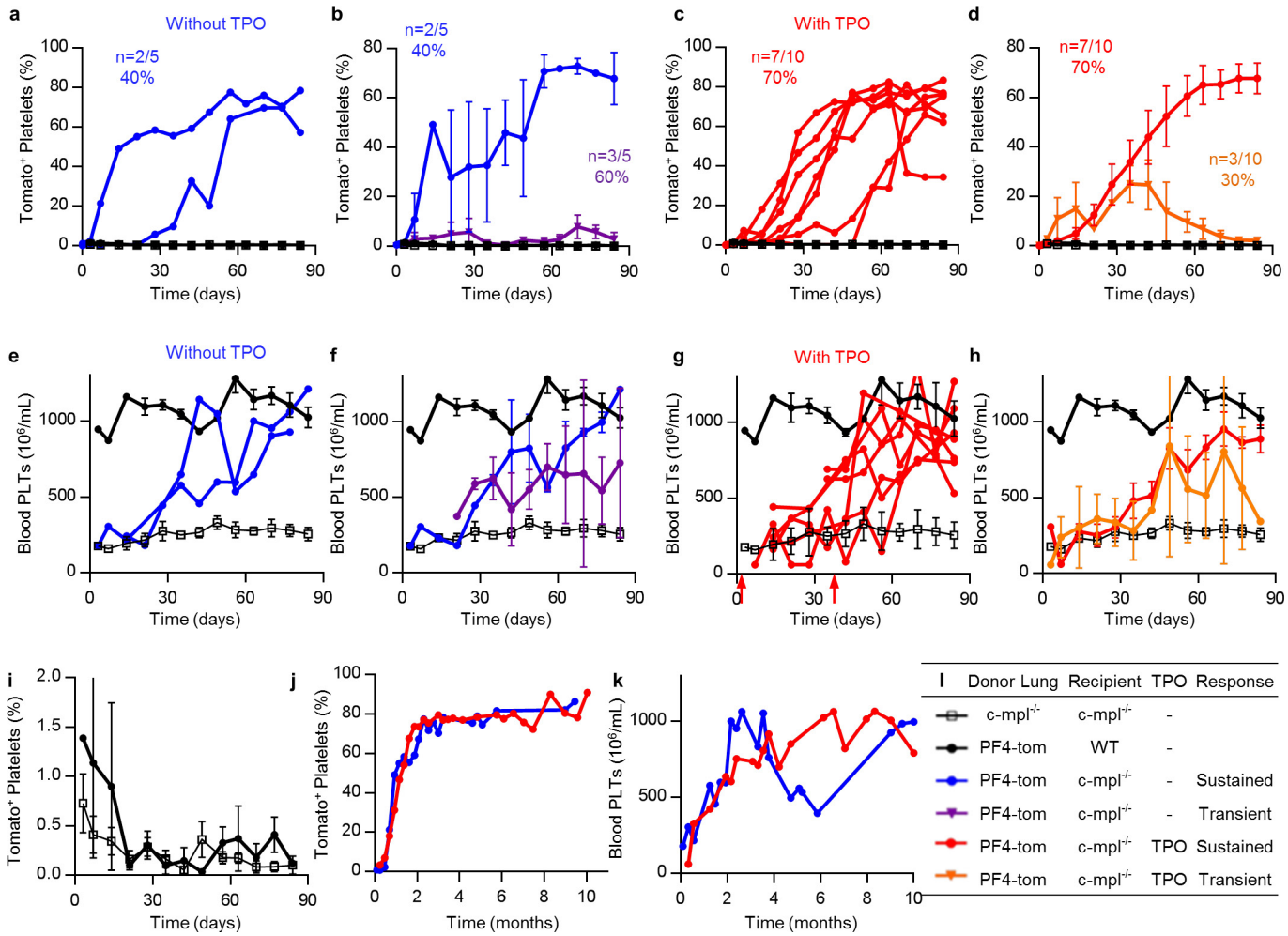


**Extended Data Figure 5 | Platelet reconstitution after lung transplantation with or without TPO injection.** Blood was collected from the mandibular vein every week following lung transplantation. After transplantation, a group of mice (red and orange) received TPO injection (250 mg $kg^{-1}$, days 3 and 40). The other group was left untreated (blue and purple). Some mice in each group showed sustained platelet production for more than 3 months (blue and red). In the other mice (purple and orange), the platelet production was lower and transient (less than 3 months). The percentages of mice in each group are indicated. Data from individual mice (**a**, **c**, **e**, **g**) or group averages (**b**, **d**, **f**, **h**) are plotted. **a**–**d**, **i**, **j**, Percentage of donor-derived platelets. Percentage was analysed by FACS, counting the tomato$^+$ platelets (CD41$^+$ $FSC_{small}$ gate). **e**–**h**, **k**, Overall platelet counts in the peripheral blood. **j**, **k**, Plots from mice with 10 months of sustained platelet production. **i**, Percentage of tomato$^+$ platelets in control lung transplants ($n = 4$–6). **l**, Colour code for the different lung transplant groups according to lung origin (donor), recipient mouse, treatment received (with or without TPO) and observed response (sustained or transient).

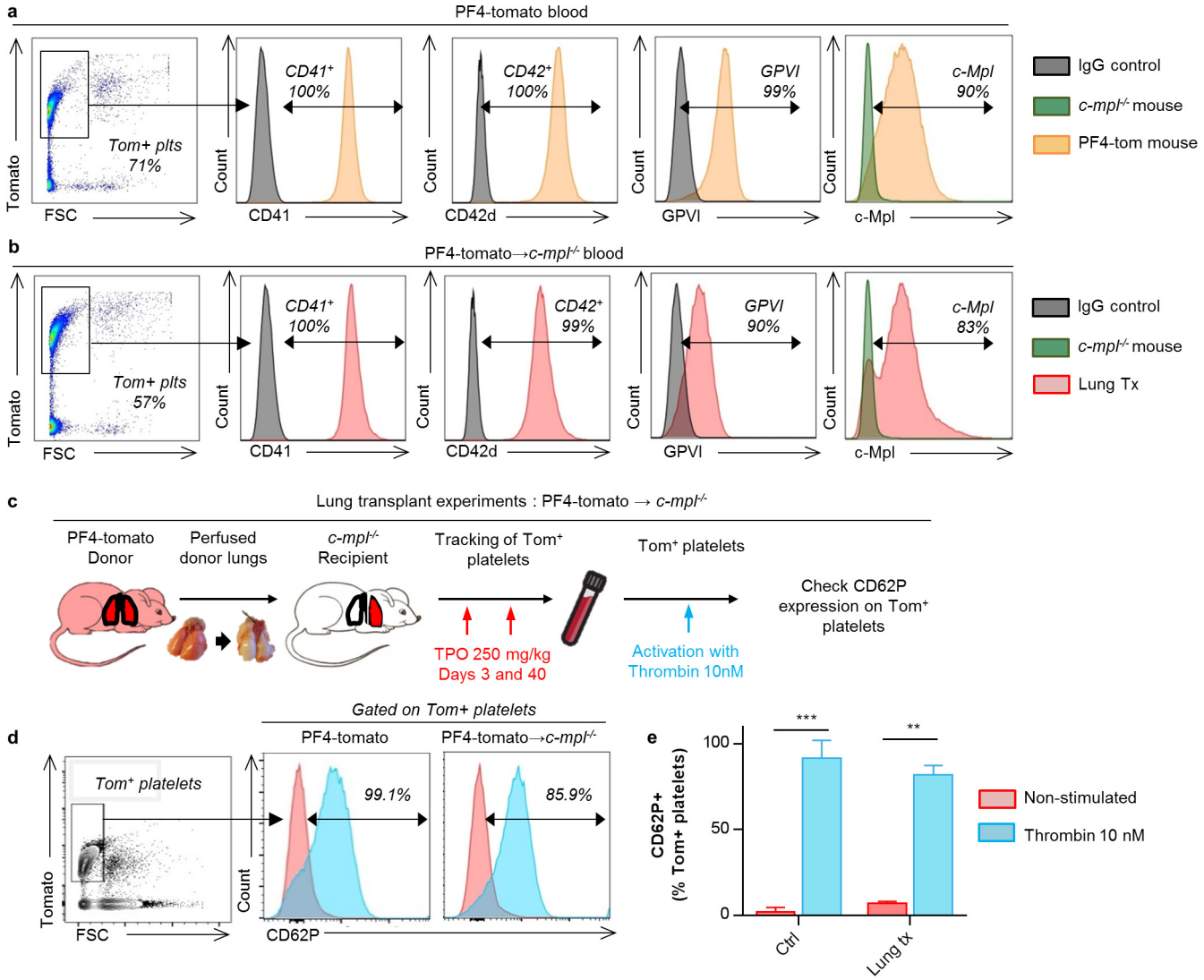


**Extended Data Figure 6 | Characterization of platelets produced after lung transplantation. a**, **b**, Flow cytometric analysis of tomato$^+$ platelets observed in the blood and stained with antibodies against CD41, CD42d, GPVI and c-Mpl. Blood from PF4-tomato mice (**a**) or *c-mpl*$^{-/-}$ mice that had received PF4-tomato lung transplants (**b**). **c**, Experimental schema for platelet activation. **d**, Flow cytometric analysis of tomato$^+$ platelets after stimulation with thrombin (10 nM) stained with antibody against CD62P. **e**, Percentage of CD62P$^+$ platelets before and after thrombin activation. Ctrl, PF4-tomato; Lung tx, PF4-tomato lungs transplanted into *c-mpl*$^{-/-}$ mice. Mean ± s.d. are presented ($n = 2$–3 mice per group). Unpaired *t*-test: $^{**}P < 0.01$, $^{***}P < 0.001$

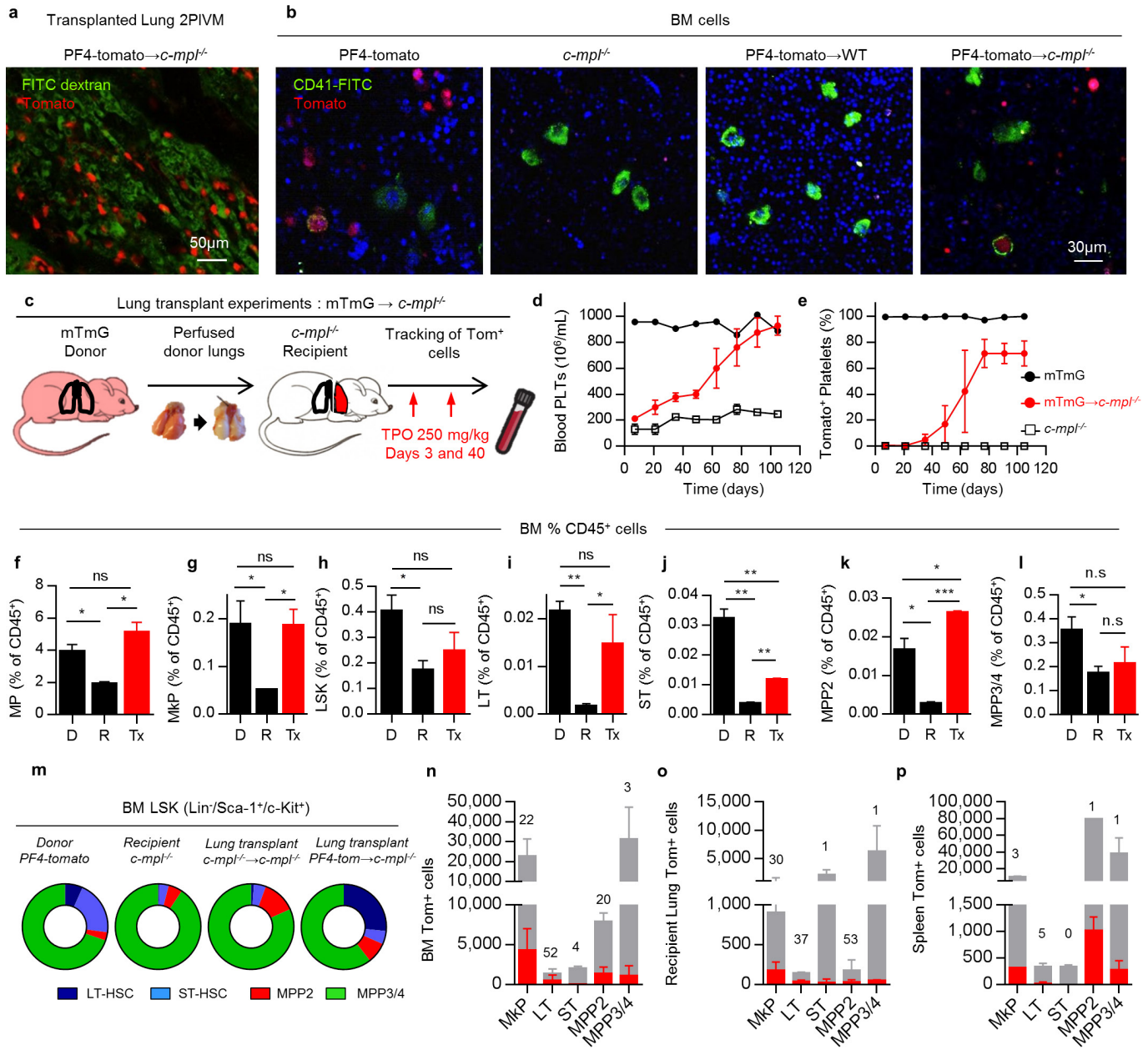


**Extended Data Figure 7 | Lung and bone marrow analysis of transplanted mice.** Mice with sustained production of lung-derived platelets were killed at least 3 months after lung transplantation. **a**, Representative 2PIVM image of a PF4-tomato lung after transplantation into a *c-mpl*$^{-/-}$ mouse. **b**, Representative 2PIVM image of flushed bone marrow cells from PF4-tomato and *c-mpl*$^{-/-}$ mice, and wild-type and *c-mpl*$^{-/-}$ mice transplanted with PF4-tomato lungs. **c**, Experimental schema for transplantation of mTmG lungs into *c-mpl*$^{-/-}$ mice. Blood was collected from the mandibular vein every 2 weeks to test for donor-derived platelets (tomato$^{+}$ platelets) and measure overall blood platelet counts. **d**, Percentage of donor-derived platelets analysed by FACS counting of tomato$^{+}$ events in the CD41$^{+}$ FSC$^{small}$ gate. **e**, Platelet counts in peripheral blood determined by CBC. **d**, **e**, Mean ± s.e.m. are presented. **f**–**l**, Bone marrow cells from mTmG mice (D), *c-mpl*$^{-/-}$ mice (R), or *c-mpl*$^{-/-}$ mice transplanted with mTmG lungs (Tx) that showed sustained donor-derived platelet production for 3 months were analysed. Population frequencies within the CD45$^{+}$ compartment were measured for myeloid progenitors (**f**, MP: Lin$^{-}$ Sca-1$^{-}$ c-Kit$^{+}$), MkPs (**g**), LSK cells (**h**, Lin$^{-}$ Sca-1$^{+}$ c-Kit$^{+}$), LT-HSCs (**i**), ST-HSCs (**j**), MPP2s (**k**) and MPP3/4s (**l**). **m**, Population frequencies within the LSK compartment from indicated groups. **n**–**p**, Total cell populations (grey), donor origin tomato$^{+}$ cells (red), and per cent tomato$^{+}$ cells (above bars) in bone marrow (**n**), recipient native lung (right lung; **o**) and spleen (**p**). Mean ± s.d. are presented ($n = 2$–3 mice per group). Unpaired *t*-test: $^{*}P < 0.05$, $^{**}P < 0.01$, $^{***}P < 0.001$.

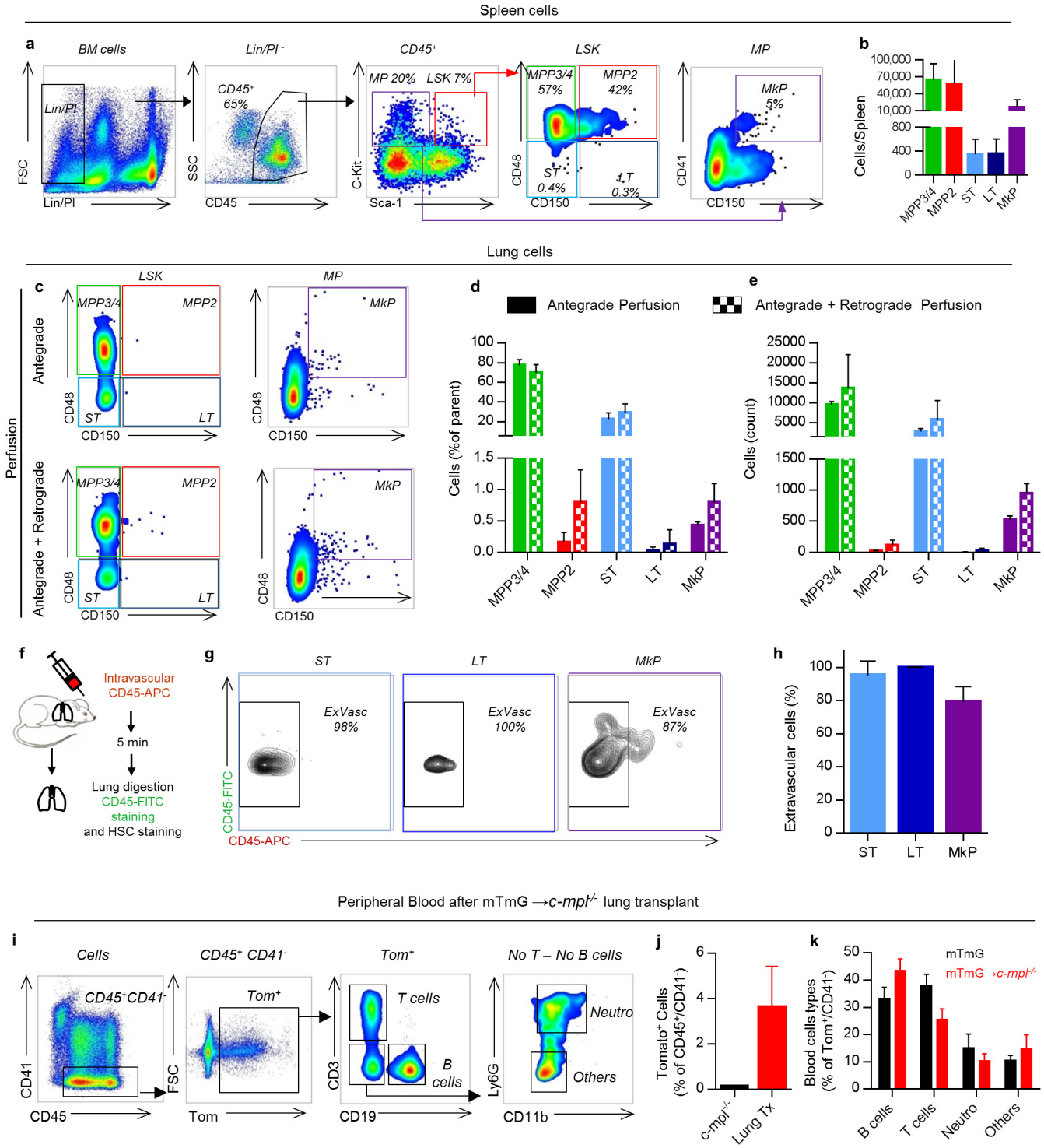


**Extended Data Figure 8 | Lung haematopoietic progenitors are extravascular and have multi-lineage capabilities. a**, Representative spleen FACS plots of haematopoietic progenitors within the LSK compartment and the myeloid progenitor compartment ($Lin^-$ $Sca\text{-}1^-$ $c\text{-}Kit^+$). **b**, Cell counts of haematopoietic progenitor populations in the spleen ($n = 6$). **c**–**e**, Lungs were perfused before digestion. **c**, Representative FACS plot of LSK and myeloid progenitor compartments with anterograde perfusion and with or without retrograde perfusion. **d**, **e**, Frequencies (**d**) and cell counts (**e**) of lung haematopoietic progenitor populations ($n = 3$). **f**–**h**, CD45-APC mAb was injected intravenously via the tail vein 5 min before lung digestion and staining with CD45-FITC mAb. **g**, Haematopoietic progenitor populations were examined for labelling with injected CD45 mAb by flow cytometry. **h**, Percentage of $CD45\text{-}FITC^+$ cells positive or negative (extravascular cells) for the intravenous CD45-APC mAb ($n = 3$–$6$). **i**–**k**, Peripheral blood was analysed 2–3 months after transplantation of mTmG lungs into $c\text{-}mpl^{-/-}$ mice. **i**, Representative FACS plot of blood cell analysis. **j**, Percentage of lung-derived cells ($Tom^+$ $CD41^-$) in the blood after transplantation. **k**, Percentage of B cells ($CD19^+$), T cells ($CD3^+$) or neutrophils ($CD11b^+$ $Ly6G^+$) in the lung-derived cells ($Tom^+$ $CD41^-$). Mean ± s.e.m. are presented ($n = 5$ mice per group).

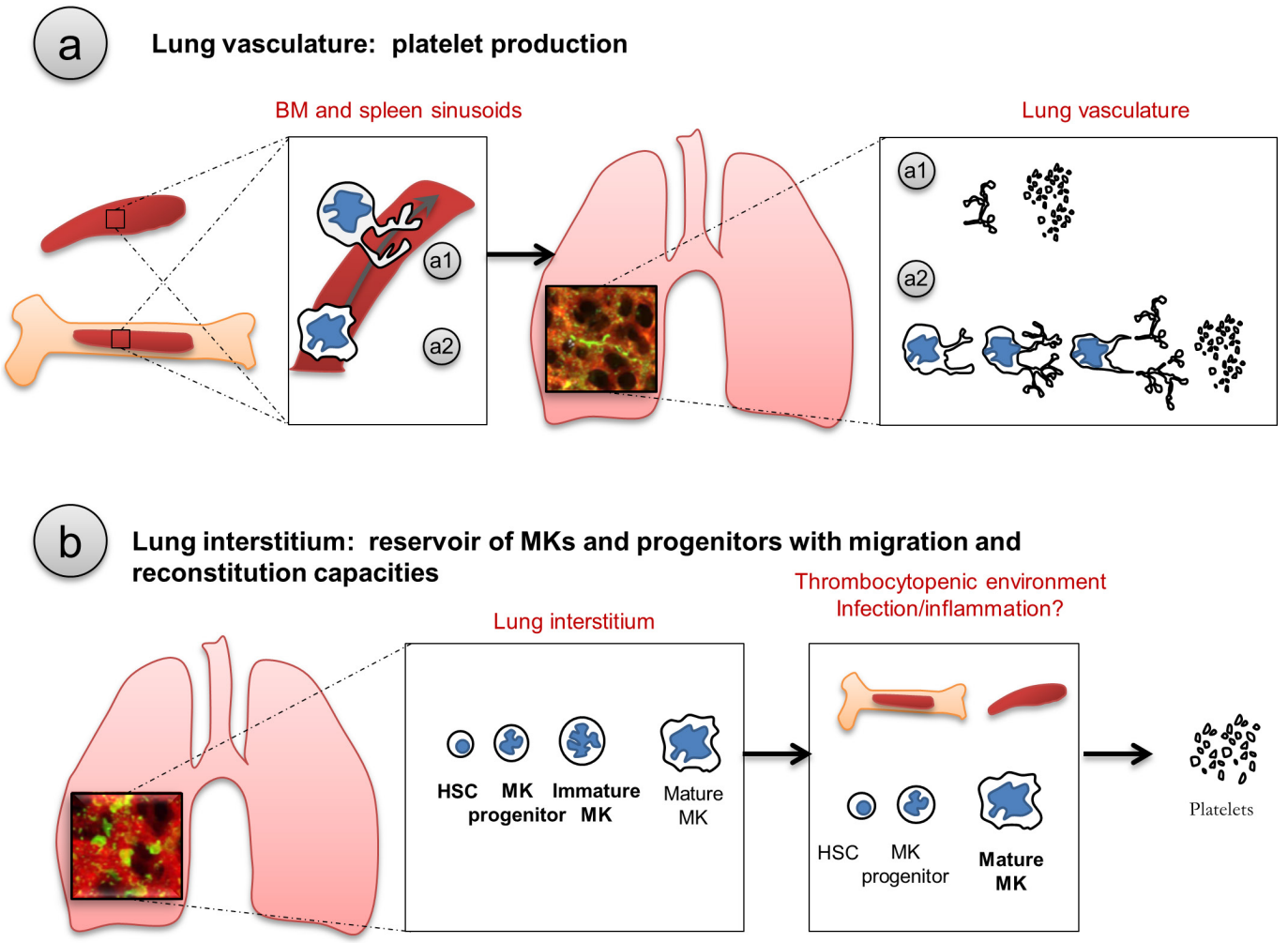


**Extended Data Figure 9 | Proposed schema of lung involvement in platelet biogenesis.** The role of the lungs in platelet biogenesis is twofold and occurs in two different compartments. **a**, Platelet production in the lung vasculature. After being released from the bone marrow or the spleen, proplatelets (**a1**) and megakaryocytes (**a2**) are retained in the lung vasculature, the first capillary bed encountered by any cell leaving the bone marrow, where proplatelet formation and extension and final platelet release are observed. **b**, Mature and immature megakaryocytes along with haematopoietic progenitors are found in the lung interstitium. In thrombocytopenic environments, haematopoietic progenitors from the lung migrate and restore bone marrow haematopoietic deficiencies.

**Extended Data Table 1 | Variables used to calculate the number and percentage of platelets produced by the lungs**

| Variable | Name | Method | Value |
|---|---|---|---|
| Volume of lung imaged | $Volume_{observed}$ | Calculated from x, y, z dimensions | 0.07 $mm^3$ |
| Volume of adult mouse lung | $Volume_{lung}$ | Known from literature | 700 $mm^3$ |
| # MK undergoing fragmentation imaged/hour | Lung-$MK_{frag}$/hour | Measured using Imaris | |
| #Platelets released per MK | $N_{Plat/MK}$ | Calculated using Imaris | |
| Platelet life-span | LifePlat | Known from literature | 4 days |
| #Platelets in adult mouse | $Plat_{blood}$ | Known from literature | $1.5x10^9$ |
| #Platelets sequestered in spleen | $Plat_{Spleen}$ | Known from literature | One-third |